THE CORROSION FATIGUE BEHAVIOR OF NOTCHED 2024-T351 ALUMINUM

by

Steve An-Ter Chang

Thesis submitted to the Graduate Faculty of the

Virginia Polytechnic Institute and State University

in partial fulfillment of the requirements for the degree of

MASTER OF SCIENCE

in

Materials Engineering

APPROVED:

J. L. Lytton, Chairman

C. R. Houska

T. P. Floridis

December, 1977

ACKNOWLEDGMENTS

The author wishes to express his deep appreciation to

for his advice and guidance during the past year of graduate study. has provided the inspiration and the extra care to enable this thesis to be written. His many suggestions and comments have made a tremendous contribution in this work.

The author wishes to express his appreciation to the faculty and staff of the Department of Materials Engineering for their special care given to a foreign student.

The author is grateful to and for making the complicated testing-pieces which enabled this investigation to be done. Thanks are given to and

for their helps during the investigation.

Sincere appreciation is expressed to his wife, , for her encouragement throughout his graduate study and for typing this thesis.

TABLE OF CONTENTS

LIST OF FIGURES

LIST OF TABLES

I. INTRODUCTION

It is recognized that the behavior of an engineering structure in service cannot be predicted solely from the mechanical behavior deduced from simple tests such as the tensile test or the fatigue test. One reason for this is that the nature of the service environment frequently includes corrosion effects combined with states of stress not encountered in many laboratory tests. On the other hand, the study of notched specimens combined with corrosion fatigue can yield significant information about the behavior of metals under critical circumstances.

The principal value of notched tensile testing for engineering purposes arises from the ability of such tests to distinguish between "notch ductile" and "notch brittle" behavior in notched members under tensile load[1]. Numerous investigations have been conducted on notched tensile test bars[2,3]. However, the analysis of these tests has been limited. The problem of assessing the effect of a notch on the fatigue properties of a material has been the subject of a considerable amount of work[4,5,6]. Notched fatigue tests using the rotating-beam method have been carried out to predict the value of K_f, the fatigue stress-concentration factor, using Neuber's notch rule[6,7,8]. Corrosion fatigue tests have generally shown that corrosive atmospheres severely effect the fatigue behavior of metals[5,9,10].

Alumimum alloy 2024-T351 possesses a desirable combination of high strength-to-weight ratio and reasonable ductility. It also combines good corrosion resistance with good toughness. The purpose of this investigation was to study the fracture characteristics of aluminum

2024-T351 using the notched tensile test and the notched fatigue test under circumstances where salt-water corrosion occurs.

Fracture characteristics were correlated with the appearance of the fracture surfaces as received in the scanning electron microscope.

II. LITERATURE REVIEW

A. Notch Characteristics of Metals

The static tension test performed on a circumferentially notched cylindrical bar has attracted considerable interest for the evaluation of metals for service. It has been recognized that the ordinary tension test is frequently incapable of predicting the behavior of a material in service, especially if service conditions entail embrittling factors such as stress raisers. Under these circumstances, the notched tensile test is a better criterion of service performance than the unnotched tension test[11].

It is recognized that the stress and strain relations in deeply notched, plastically stretched bars are very complex. The high longitudinal stress at the root of the notch and the transverse tension in the notched section affect the shape of the stress-strain curve significantly. When the stress at the bottom of the notch reaches the yield strength of the metal, plastic flow occurs in that region. The transverse tension as it is superimposed upon longitudinal tension raises the stress required to produce a given amount of plastic flow. Thus the entire stress-strain curve tends to be higher than would be the case if no transverse stress were present[12].

Two fundamental effects occur in the notched tensile test: (1) the effect of stress concentration, and (2) the effect of triaxiality. These will be briefly reviewed in this section.

1. Stress Concentration

A maximum longitudinal stress occurs at the locations of maximum curvature (minimum radius) of the surface. The ratio between this maximum stress and the nominal stress derived from the elementary theory of elasticity is called stress concentration. Stress-concentration factors for practical problems are usually determined by experimental methods[13]. Photoelastic analysis from models is the most widely used technique[14]. Peterson has collected much information on stress concentration in machine parts[15]. Several factors affect the stress distribution at the notched section of a notched round bar. These are eccentricity of loading, surface condition, notch tip radius and plastic strain[12,16,17].

Eccentricity of loading will produce a lower stress in a tensile test[12]. Consequently, it must be accepted that the stress concentration has been affected. In this investigation, two universal joints have been used to avoid eccentricity of loading as far as possible. Surface conditions caused by machining have been studied by Dana and Aul[2,3]. According to these authors, machining of the notch results in severe cold working of the metal at the notch bottom. Caution must therefore be taken in machining every specimen, so that each specimen will get the same degree of cold working. Variation of the notch radius has been thought to be a partial cause of the scattering of testing results through variations of stress concentration factor. Also, it has been found that there is little change in ductile properties for notch radius values ranging from zero to 1/22 inch[12] i.e. for a sharp notch. Consequently, if notch tip radius is chosen between zero and 1/22 inch, the variation in stress concentration factor for ductile metals will be

minimized. Plastic strain has been found to have a predominant effect on stress concentration[16]. The stress concentration factor is reduced enormously by a few percent of plastic strain, and will goes to unity when plastic strain is larger than 2 percent.

2. Triaxiality

Many factors are known to favor the brittle behavior of metals, such as a very low temperature[18] or a corrosive atmosphere[5,10,19]. However the only feature which appears to be common to all the brittle metal failures that have been observed, excluding fatigue failures, seems to be the presence of a triaxial tension-stress state. In other words, tension in all three directions will be invariably found if a brittle fracture occurs. In addition, most of these failures have occurred at the location of stress concentrations as has been discussed in the last paragraph.

The triaxiality depends primarily upon the notch depth, i.e., the percentage of cross-sectional area removed by notching. Other conditions, such as notch tip radius and plastic strain, were found to have a considerable effect upon the stress-concentration factor, but apparently have only a negligible effect upon the triaxiality in certain ranges[20].

According to Sachs and Lubahn[16], the degree of nonuniformity of any distribution of stress, such as the distribution of longitudinal stress or transverse stress will change progressively with such variables as plastic strain and will approach a condition of uniform stress as a limit. Under these circumstances, average longitudinal

stress and average transverse stress can be used to calculate the triaxiality. They defined triaxiality as the ratio between the average radial stress, i.e. one of the two transverse stresses, S_T, and the average longitudinal stress, S_L, in the notched section of a cylindrical test bar subjected to longitudinal tension. From the assumption of plastic behavior, the transverse stress, S_T, is determined by the following relation

$$S_L - S_T = S_0 \qquad (1)$$

in which S_0 represents the unnotched tensile yielding strength and the two principal stresses normal to the longitudinal stress are equal from the assumption of rotational symmetry. Under these conditions, the triaxiality at the point of maximum load becomes simply

$$\frac{S_T}{S_L} = 1 - \frac{S_0}{S_L} \qquad (2)$$

The triaxiality of specimens of different notch depth for the aluminum alloy 2024-T351 were calculated from this formula.

B. Fatigue Properties of Metals

Fatigue strength is probably the most sensitive of the engineering properties to manufacturing processing, because the imperfections produced have a vital effect on fatigue performance. Man's inability to manufacture the material perfectly (flawlessly, free of residual stresses, etc.); his inability to fabricate the structures from the materials without using somewhat primitive joining methods involving

geometrical and metallurgical notches, etc.; and finally, his inability to define completely the environment (loadings, etc.) that the structure must experience in its lifetime all combine to cause the problems associated with fatigue life prediction. Fatigue failures generally start as minute surface cracks which grow under the action of a fluctuating stress until a dominant crack attains critical size, causing failure. The stress necessary to initiate fatigue cracks is often less than that required to cause gross plastic deformation of the material. There is often little relief of the stress concentration at discontinuities, and cracks will generally start at such stress-raisers.

1. Fatigue Stress Concentration

Fatigue strength is seriously reduced by the introduction of a stress raiser such as a notch or hole. The effect of a notch on the fatigue strength of a part varies considerally with material and notch geometry and is usually less than the effect which would be predicted by use of the theoretical stress concentration factor. The concept of notch sensitivity is defined to denote this general phenomenon[8]. It is usually expressed by the notch-sensitivity index q given by

$$q = \frac{K_f - 1}{K_t - 1} \qquad (3)$$

where q = notch-sensitivity index,

K_f = the ratio of unnotched fatigue limit to notched fatigue limit, and

K_t = the theoretical stress-concentration factor.

Equation (3) was chosen so that a material which experiences no reduction in fatigue strength due to a notch has an index of zero, while a material in which the notch has its full theoretical effect has a value of 1. According to Peterson[21], the notch-sensitivity index q is approximately 0.18 for an aluminum alloy with a notch radius of 0.003 inch whose theoretical stress-concentration factor K_t, is equal to 5.4[15]. The corresponding notch-fatigue factor, K_f, can be calculated from equation (3), and is equal to 1.80, i.e., the unnotched fatigue strength is about 2 times of notched fatigue strength. In general, typical K_f values can be useful in estimating the true notch fatigue strength, if the unnotched fatigue strength is already known.

2. Fatigue Crack Initiation and Propagation

Fatigue failures are usually caused by the initiation and cyclic growth of one or more cracks from areas of stress concentration. The rate at which the crack grows depends primarily on the material specimen configuration, the cyclic loads applied, and the environmental condition.

Two approaches to the problem of the propagation or growth of a fatigue crack have been accepted: (1) once a crack is initiated, it propagates very rapidly due to the high stress-concentration set up at the tip of the crack, and (2) a crack forms at as early as 10 percent of the total life and then spends the remaining 90% in propagating[22]. However, it has been shown in both cases that the processes of the fatigue failure can be divided into three stages. (1) Crack nucleation (2) Crack propagation (3) Final failure. The last stage will not be discussed here.

Several microstructural mechanisms of crack nucleation and propagation[23,24,25,26] have been applied to explain crack nucleation and crack growth. In this mechanism, dislocation slip movements and plastic deformation caused by cyclic stress contributed to the phenomena of crack tip nucleation and crack growth. The basic idea of these dislocation mechanisms is illustrated by Figure 1 [23]. It is true that any factor affecting dislocation movement will affect fatigue crack nucleation and propagation. For example, stress condition, inclusion content, and the presence of solute atoms all are important factors in fatigue cracking.

3. Corrosion Fatigue

The fatigue strength of materials is often more sensitive to the chemical environment than are other mechanical properties. The simultaneous action of a corrosive environment and cyclic stress is referred to as corrosion fatigue. The combination of a mild corrosive agent and alternating stress is much more damaging than either one separately. The frequency of load cycling, which has only a minor effect in conventional tests, has a marked effect on the fatigue life under corrosion fatigue conditions. Although corrosion occurs whenever the corrosive environment exists in unstressed specimens, the corrosion rate is increased enormously under the action of cyclic stress.

Corrosive environments are usually in the form of liquids, vapors, or gases which surround the member being fatigued. The method of producing corrosion in a fatigue test varies. A stream of 3% salt water has been used as the corrosive agent in this study.

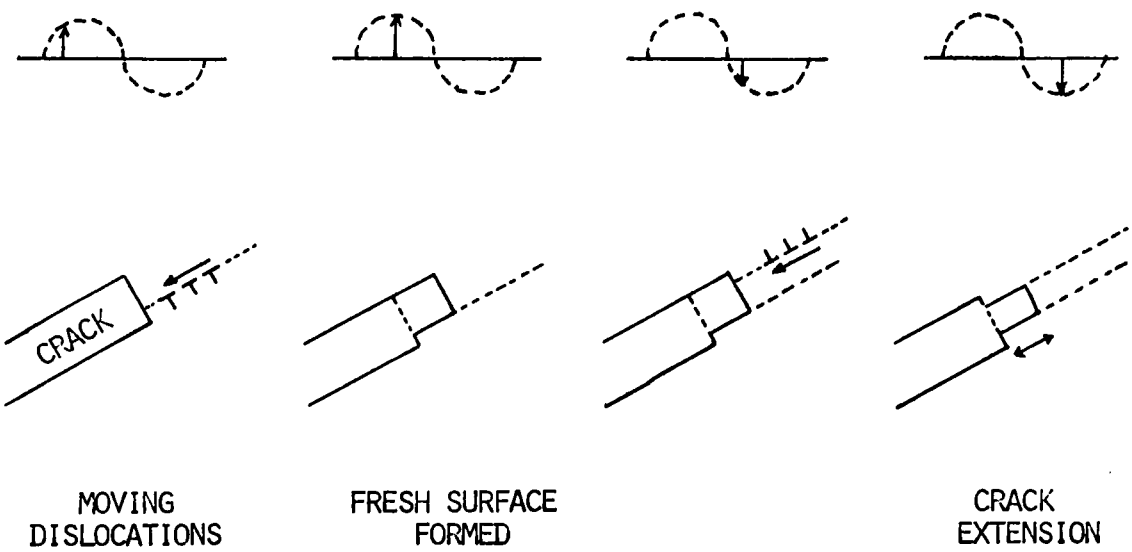

Figure 1. Four subsequent stages of simple model of crack extension during one cycle.
(after Schijve (23))

The usual fatigue test conducted in air is influenced by oxygen or moisture, therefore, represent a measure of corrosive fatigue too. The majority of fatigue failure are, in fact, corrosion fatigue failures unless the fatigue test conducted in absolute vacuum[27,28].

In general, corrosion fatigue should not be confused with stress corrosion cracking. All metals which are susceptible to corrosion are susceptible to corrosion fatigue in any corrosive environment[10]. Stress corrosion cracking, on the other hand, occurs in alloys in very specific environments, and occurs under static stress rather than dynamic stress. Factors important in crack initiation and propagation in corrosion fatigue processes are listed in Figure 2[29]. In the electrochemical mechanisms of corrosion behavior, O_2, H_2O and Cl^- are accelerators of corrosion fatigue crack. In air fatigue tests, oxygen and moisture control the corrosion behavior. In salt water corrosion tests, 3% N_aCl is used to ensure a maximum corrosion rate[10,29,30,31].

C. Fractography

Electron fractography has become a very useful tool in the analysis of service failures. It frequently permits the unambiguous identification of fatigue striations, intergranular fracture, transgranular fracture, dimples, or cleavage facets which are known to be caused by specific conditions of stress and environment[32,33,34].

Two types of electron microscopes are presently in common use to study fracture surfaces: (1) the scanning electron microscope, and (2) the transmission electron microscope. Both of them possess a large depth of field, a high resolving power, and a large range of magnification.

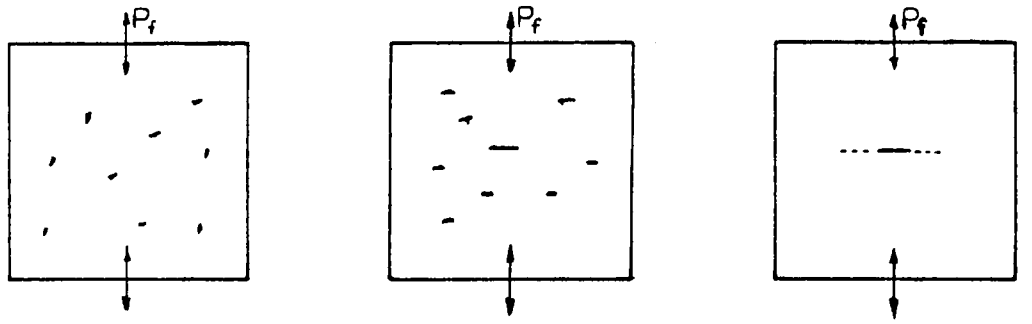

1. Corrosive attack under cyclic loading.
2. Generation of a crack of initial size.
3. Environmentally enhanced fatigue-crack propagation.

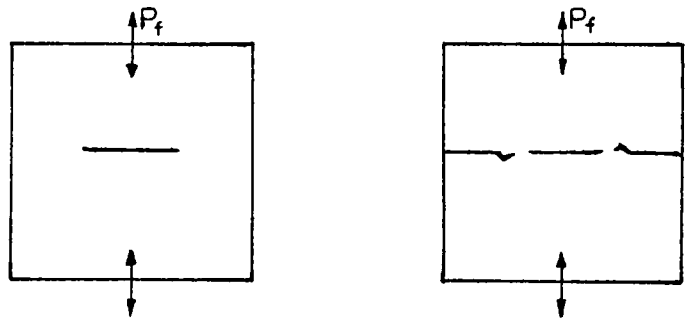

4. Stress intensity dominated fatigue-crack growth.
5. Unstabled fracture.

Figure 2. Factors important to initiation and propagation in the corrosion fatigue process.

The scanning electron microscope permits, with limited resolution, the direct study of the fracture surface itself. This has the advantage that one can observe directly the external form of real objects, such as complex fracture surfaces, at high magnification. The transmission microscope necessitates the use of thin replicas taken from fracture surfaces[34].

As the fracture surfaces are observed at increasingly higher magnifications, the extremely complex nature of the fracture features or the fracture path become more and more apparent. Study of the fracture features in aluminum alloys can be classified into the following: (1) micro-void coalescence (2) cleavage and quasi-cleavage and (3) fatigue.

In most ductile materials, fracture involving the formation and coalescence of micro-voids is of major importance[35,36]. The initiation of the micro-voids is dependent upon the existence of some heterogeneities or defects originally present in the material or created during plastic deformation. Each micro-void is a fracture surface in itself, initially isolated from the other voids. During plastic flow, these voids continue to grow and then coalesce with neighboring voids. So-called Dimpled rupture is then produced.

Cleavage is defined as the separation of a crystal along certain crystallographic planes. Screw dislocations either present in the crystal or created by plastic deformation at the tip of the advancing crack, are considered to be responsible for the formation of cleavage steps on the fracture surface[32,37]. Quasi-cleavage is used to distinguish the facets caused by precipitate and nonmetallic inclusions from

the crystalline cleavage planes[32].

Fatigue fracture surfaces in an aluminum alloy examined by optical microscopy shows dull and bright regions. The examination of the same surface by electron microscopy shows that the brighter zones are composed of a series of regular striations and the duller zones are made up of the dimples characteristic of a rapid, plastic fracture by micro-void coalescence. The striations of the bright zones are clearly resolved and, in the case of a fatigue test under a constant stress amplitude, the spacing of the striations is locally very uniform. Many investigators have studied the mechanisms of fatigue-crack propagation through measurement of the spacing of these striations[38,39].

The use of the scanning electron microscope provides for stereoscopic microfractography which is very useful in studying the fracture surface of metals. The obvious advantage of stereomicrography is that the observer sees a three-dimensional view of the specimen surface. This can eliminate much of the confusion that can result from ambiguous interpretation of the surface topography in a single micrograph.

III. EXPERIMENTAL PROCEDURE

For the experimental investigation of the fracture properties of notched round bar of aluminum alloy. Commercial alloy 2024-T351 was selected. The reasons to choose this material are due to (a) 2024-T351 is widely used, so the work will have real practical value, and (b) 2024-T351 is very tough, and so difficult to evaluate its fracture characteristics by current standard procedured such as ASTM method E399. The specimens were prepared, fatigue-precracked then go to tensile test and examine under scanning electron microscope.

A. Materials Investigated

Two rods of commercial aluminum alloy type 2024-T351 were obtained from Aluminum Company of America, each 3/4 inch diameter and 12 feet long. The designation T351 is applied to the heat-treatable alloy 2024 when it is stress-relieved by 2% cold stretching after solution heat treatment. This treatment is followed by a natural aging at room temperature and results in additional precipitation of $CuAl_2$ particles to produce maximum room temperature strength. The chemical composition and mechanical properties of 2024-T351 are given in Table I[40].

The rods were cut into appropriate lengths and marked with consecutive serial numbers. Each number denotes both the rod number and the number of the specimen from each rod, e.g. specimen 2-1 would be the first specimen from the second rod.

B. Specimen Preparation

Two types of specimen were used in this investigation: (1) tensile test specimens, and (2) fatigue test specimens (Figure 3).

TABLE I

Chemical Composition and Mechanical Properties of Aluminum Alloy 2024-T351

Element	Cu	Mg	Mn	Si	Fe	Cr	Zn	Al
Percent by weight	4.4	1.5	0.6	0.5	0.5	0.1	0.2	Remainder

Yield Strength	Tensile Strength	Elongation	Area Reduction
53000 psi	69600 psi	18%	26.4%

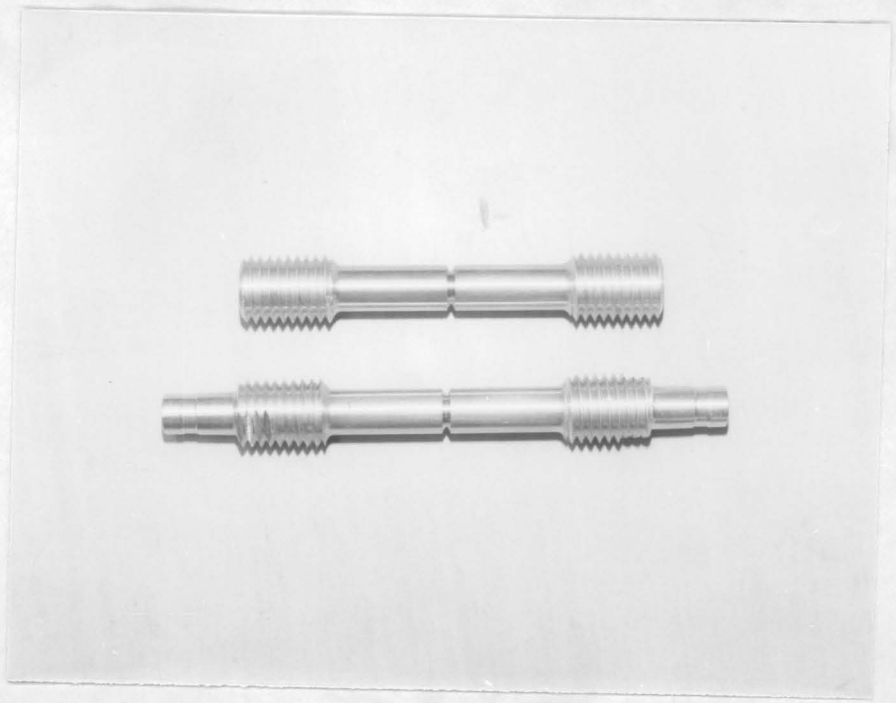

Figure 3. Types of Specimen Investigated.

The standard 0.500 inch (12.5 mm) diameter round tensile test specimens shown in Figure 3 is in accord with industrial standards[41]. The shape of the threaded ends of the specimen outside of the gage length were suitable to fit the grips of the Instron testing machine so that the loads would be applied axially. To furthur ensure axiality of loading, two universal joints were used.

In the middle of each bar, a circumferential V-notch was cut. The V-groove of each specimen was cut on a lathe using initial cuts of 0.010 inch per revolution, followed by three cuts of 0.002 inch per revolution, and four final cuts of 0.001 inch per revolution. These final cuts were designed to minimize the difference between each groove and to minimize the residual stress on the notch tip. During machining, a cutting fluid was used to minimize heat generation. Since the notch configuration is an important part of this investigation, a microprojector was used to examine each specimen made to ensure its dimensional accuracy. The angle of notch used was sixty degrees. The notch tip radius of the specimens was 0.003 inch.

As seen in Figure 3, fatigue test specimens were made so that they could be pulled in tension in the Instron testing machine following prior fatigue in the R. R. Moore machine.

In preparing these specimens according to ASTM standards[42,43], one should avoid: (1) overheating the specimens during machining, (2) cold working the material at the surface of the specimen, and (3) repeated stressing of the specimen during machining by excessive vibration. Also, it was necessary to insure that the grip ends were coaxial so that the

specimen would run smoothly in the machine. The circumferential V-notch of 50% notch-depth was then cut into the specimen to provide the desired stress-concentration. The specimen profile is shown in Figure 3.

C. Tensile Test

An Instron testing machine of 20,000 pound capacity was used for the tensile tests in this investigation. The specimen grips used for the notched, 0.500 inch diameter, threaded-end specimen is shown in Figure 4. A universal joint was used at each end of the specimen to ensure axial tensile stress within the gage length. Other investigators have shown that any departure from axiality may introduce bending stresses that may adversely affect the results.[12] The crosshead speed used was 0.05 inch per minute. Calibration of the machine, including calibration of the strain gage amplifier, was done prior to each test. An Instron strain gage extensometer, one inch gage length, Serial Number G-51-12, was connected to the amplifier.

The amplifier was balanced to give 0.5 inch of chart travel for each 0.001 inch of extensometer deflection. Load and strain were recorded through the X-Y chart driving amplifiers until the specimen had broken.

Notch tensile strength was calculated by dividing the maximum load, P, carried by the specimen during the test by the original cross-sectional area at the root of the notch:

$$N.T.S. = \frac{4\,P}{\pi\,d^2} \qquad (4)$$

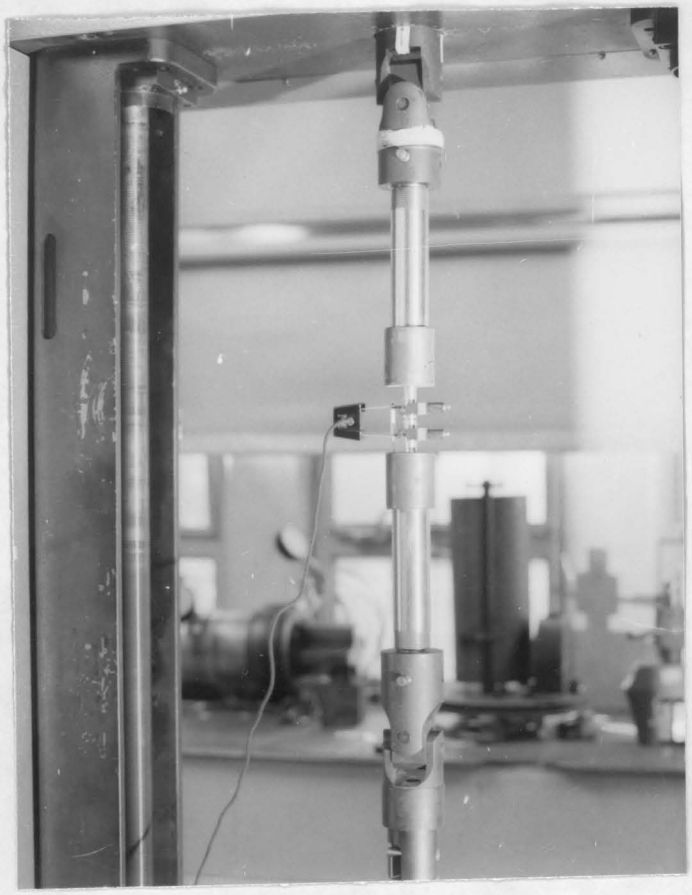

Figure 4. Overall view of the two universal joints with the extensometer on the specimen.

where N.T.S. = notch tensile strength, psi,

P = maximum load on the chart, pounds, and

d = notch diameter in inches.

As illustrated schematically in Figure 5, the notch yield strength was calculated from the recorded load-deflection curve using an offset technique. The offset used corresponded to 0.001 inch of deflection over one inch of gage length; i.e., 0.1%. Many investigators have measured notch ductility as defined from the contraction of the notched area during fracture.[1,12,17] In this study, a new parameter, ϵ_g, was used to represent notch ductility. This was taken as the apparent permanent strain at fracture, again assuming one inch of gage length (see Figure 5).

D. Prestraining

Prestraining of notched specimens for use in fatigue tests was performed at room temperature on the Instron testing machine. A 10,000 pounds tensile load cell was used, since the specimens were loaded to 6,500 pounds. The 6,500 pounds was so chosen so as to exceed the elastic limit of 50% notched specimens and produce yielding at the root of the notch. (Figure 5) It is assumed that some permanent strain occurred at the root of the notch under this load. As described in the previous section, strain was measured using the extensometer and was recorded through the chart drive amplifier. The samples were loaded to 6,500 pounds using a crosshead speed of 0.05 inch per minute, and then unloaded and removed for the fatigue test.

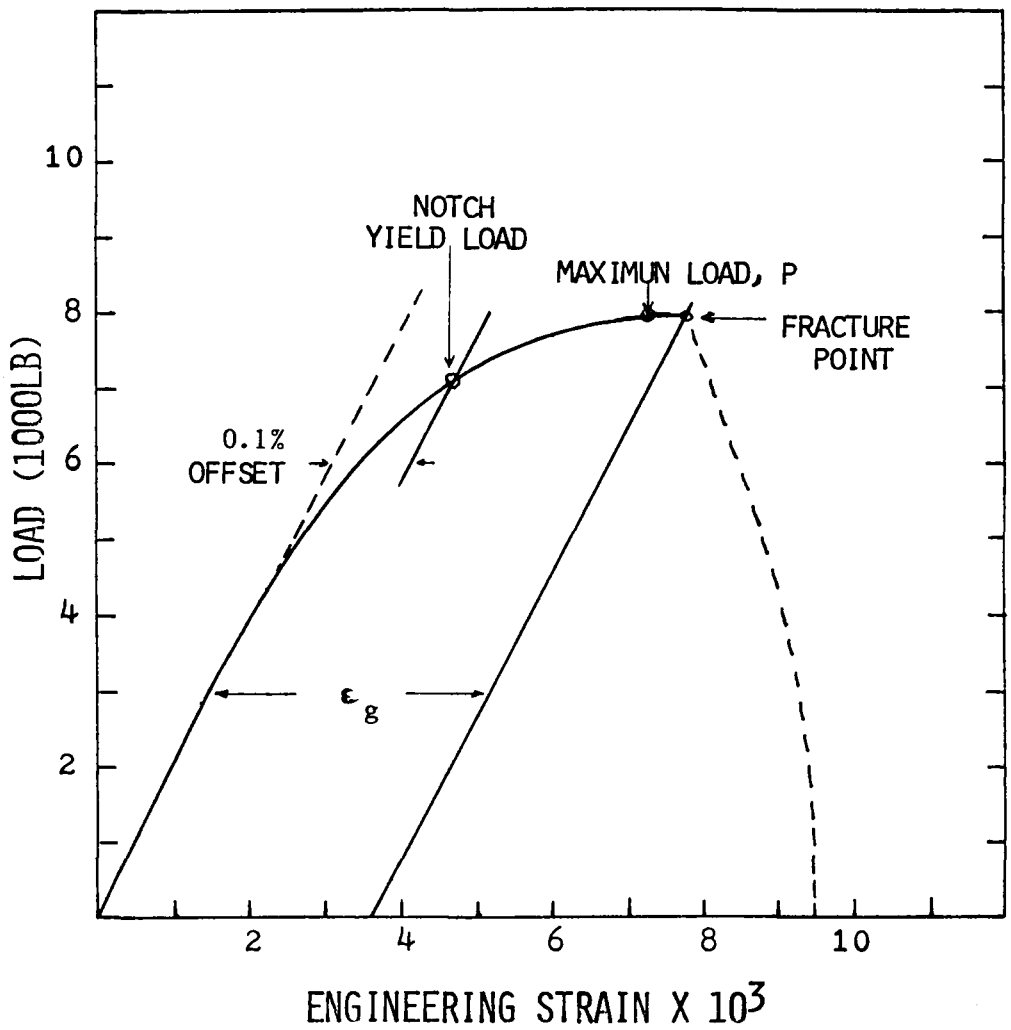

Figure 5. Schematic load-strain diagram for notched tensile tests.

E. Fatigue Test

A modified R. R. Moore type fatigue machine as shown in Figure 6 was used in this part of the investigation. The procedures used for fatigue testing of notched specimens were follows:

1. Measure the diameter of the notch to the nearest 0.001 inch.
2. Compute the load needed for a desired stress using the equation:

$$S = \frac{20.372\ (F + 11.5)}{d^3} \qquad (5)$$

where S = stress desired, psi,

F = load, pounds, and

d = notch diameter, inches.

3. Clamp the specimen to the spindles, A and B, by means of draw-in bolts. Rotate the spindle slowly to be certain the specimen and spindles run true.
4. Carefully add the weights needed and then start the machine. Immediately start to apply salt water to the notch, if needed.
5. Record the counter reading, i.e., cycles to failure after the specimen has failed.

The average frequency of the machine has been found to be 15050 $\pm$ 50 RPM. In the last few tests in this study, the revolution counter had failed and the cycles to failure were determined from elapsed time using a frequency of 15050 cycles per minute.

A three-percent salt water solution was used as corrosive agent to

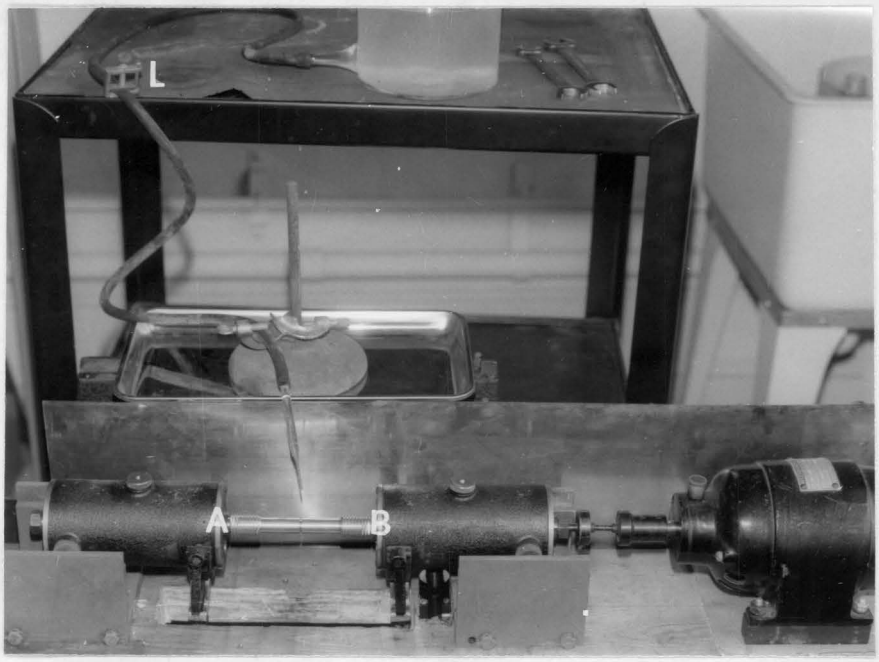

Figure 6. R-R Moore type Reverse Bending Fatigue Machine as modified for notched tensile specimens.

induce corrosion fatigue. By adjusting the stopcock (shown as L in Figure 6), it was possible to standardize the flow of salt water onto the notch of specimen to a rate of 5 ml per minute, or about one drop per second.

F. Scanning Electron Microscope

An AMR-900 Scanning Electron Microscope was used to examine the fracture surfaces of various failed specimens. The samples were cut and subsequently mounted on a small sample holder. A low-speed diamond saw was used to cut the sample at a position one quarter inch from the fracture surface. This was sufficiently removed from the fracture surface to ensure that the structure of the fracture surface would not be effected by the cutting. Silver paint was used to ground the sample to the holder. Specimens were cleaned first in mild soap solution and then acetone to remove the adhesive dust and the products of oxidation and corrosion[44]. Stereomicrographs, using a 7^{o} tilt angle, were taken when necessary to clarify the nature of the fracture surfaces.

IV. RESULTS AND DISCUSSION

Very few investigators have studied the notched properties of the aluminum alloy 2024-T351. The results of the present study reveal that the notch strength characteristics of aluminum alloy 2024-T351 are very similar to those of other heat-treatable 2024 alloys. The fatigue properties in both salt water and air of aluminum alloy 2024-T351 have been investigated and the results reported here. The surface topology following tensile rupture and fatigue fracture were studied using scanning electron microscopy.

A. Dependence of Notch Strength Characteristics on Notch Depth

Table II is a summary of the notched tensile tests performed in this investigation. Notch yield strength was defined in Figure 4 as the stress which produces 0.1% of strain over the gage length. Notch tensile strength was defined as the maximum stress tolerated by the specimen based on the notch area. Notch strength ratio was the ratio of notch tensile strength to the unnotched tensile strength of 69,600 psi. Two definitions of notch ductility were calculated and compared in the table. Also listed was the triaxility which was calculated on the basis of equation 2. In Figures 7 through 11, the notch yield strength, notch strength ratio, notch ductility, and triaxility are shown as function of notch depth for the aluminum alloy 2024-T351, respectively.

The dependence of the notch yield strength upon notch depth for very sharply notched specimens, i.e. notch radius less than 0.005 inch, is very simple if the specimen possesses sufficient ductility to exhibit a

TABLE II

Effect of Notch Depth on the Notch Characteristics of Aluminum Alloy 2024-T351

Specimen Number	Notch Depth	Notch Diameter (inch)	Notch Area (A_o) ($inch^2$)	Fracture Area (A') ($inch^2$)	N.T.S. (psi)	N.Y.S. (psi)	N.S.R.	Notch Ductility $\frac{A_o - A'}{A_o}$	Triaxility ε_g	S_T/S_L
1-1	12.5%	0.468	0.1718	0.161	66600	59370	0.96	0.0687	0.026	0.107
1-2	12.5%	0.4689	0.1727	0.1596	68330	59062	0.982	0.0759	0.0267	0.105
1-3	25%	0.433	0.1473	0.14	70283	65170	0.01	0.0495	0.0082	0.187
1-4	25%	0.4367	0.1498	0.1428	70100	63418	1.007	0.0468	0.0088	0.164
1-5	50%	0.3535	0.100	0.096	78284	75200	1.125	0.04	0.0026	0.295
1-6	50%	0.3578	0.1005	0.0969	80360	74590	1.155	0.0388	0.0025	0.287
1-7	75%	0.250	0.049	0.0508	94118	89800	1.35	-	0.0018	0.409
1-8	75%	0.2539	0.0506	0.0489	89870	88933	1.291	0.0366	0.00142	0.403
1-0	0%	-	0.200	0.162	69600	53000				

N.T.S. - Notch Tensile Strength

N.Y.S. - 0.1% Offset Notch Yield Strength

N.S.R. - N.T.S./Unnotched T.S.

maximum load during the test. In Figure 7, notch yield strength σ_y is seen to increase with increasing notch depth. As has been previously demonstrated, this increase in notch yield strength is directly related to the increasing degree of triaxiality induced by the notch[12,16,17]. The state of triaxial tension retards the development of the shear stresses needed to induce plastic flow.

The dependence of the notch strength ratio upon notch depth is shown in Figure 8. For a sharp notch in many steels, the notch strength generally increases linearly with the notch depth to a value approximately twice the tensile strength for 100-percent notch depth. This relation is shown by the dashed line in Figure 8 and was developed for heat-treated steels[12,16,17].

However, for aluminum alloys, a different behavior has been found, especially in 2024-T351 alloy[2,3]. In Figure 8, notch strength ratio falls below the dashed line with the value for 12.5% notch depth falling below 1.0. The increase of notch strength with notch depth can be understood in view of the increasing degree of triaxiality. The fact that the sharp shallow notch reduces the notch strength ratio is due to tensile instability in the aluminum alloy 2024-T351, i.e. necking occurred in the 12.5% notched specimen because of high notch ductility.

Figure 9 shows the dependence of notch ductility upon the notch depth. Two curves are shown on the figure: (1) strain gage ductility, ε_g, as previously defined herein, and (2) "area contraction" ductility, $\frac{\Delta A}{A_o}$, as defined in previous work. In this study, the area-contraction measurements were done using a stage microscope instead of the conven-

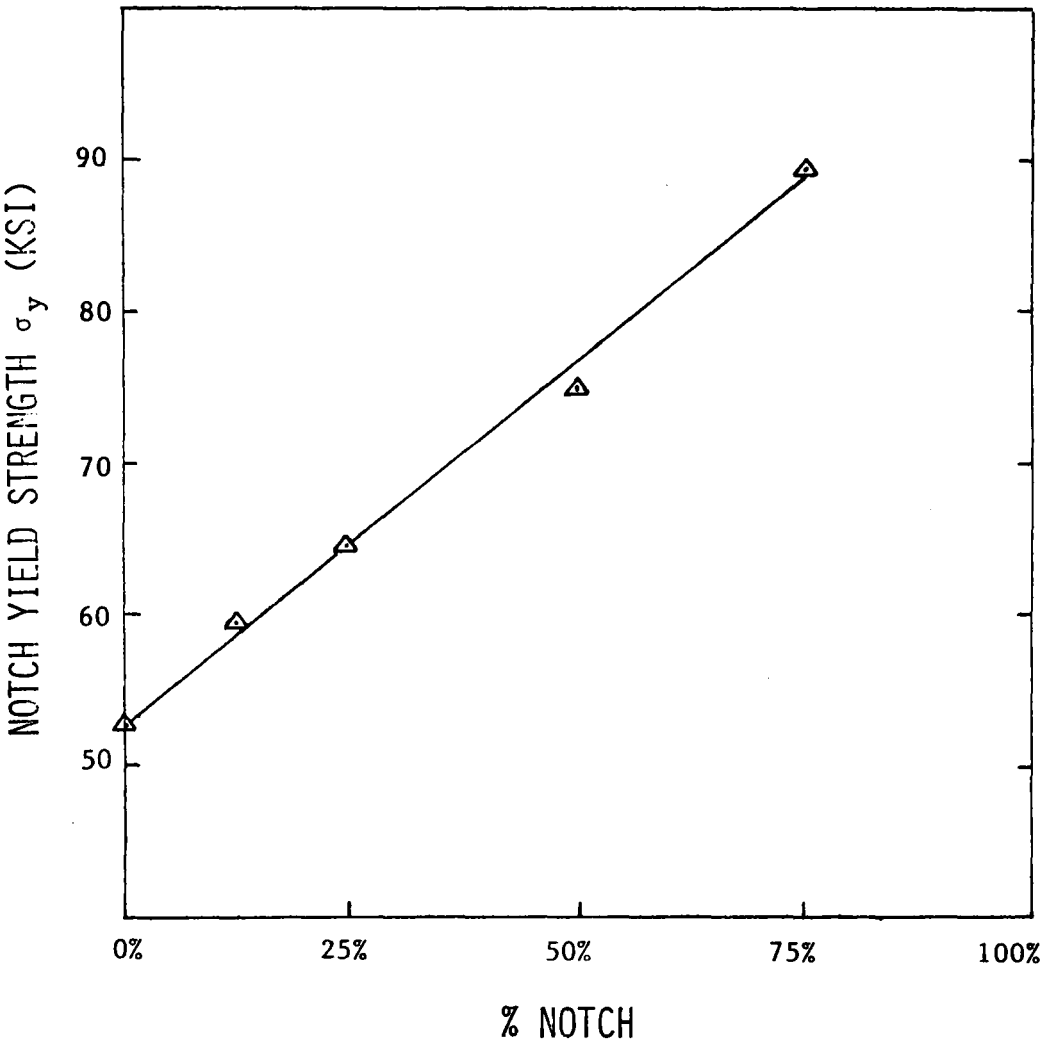

Figure 7. Effect of notch depth on the notch yield strength.

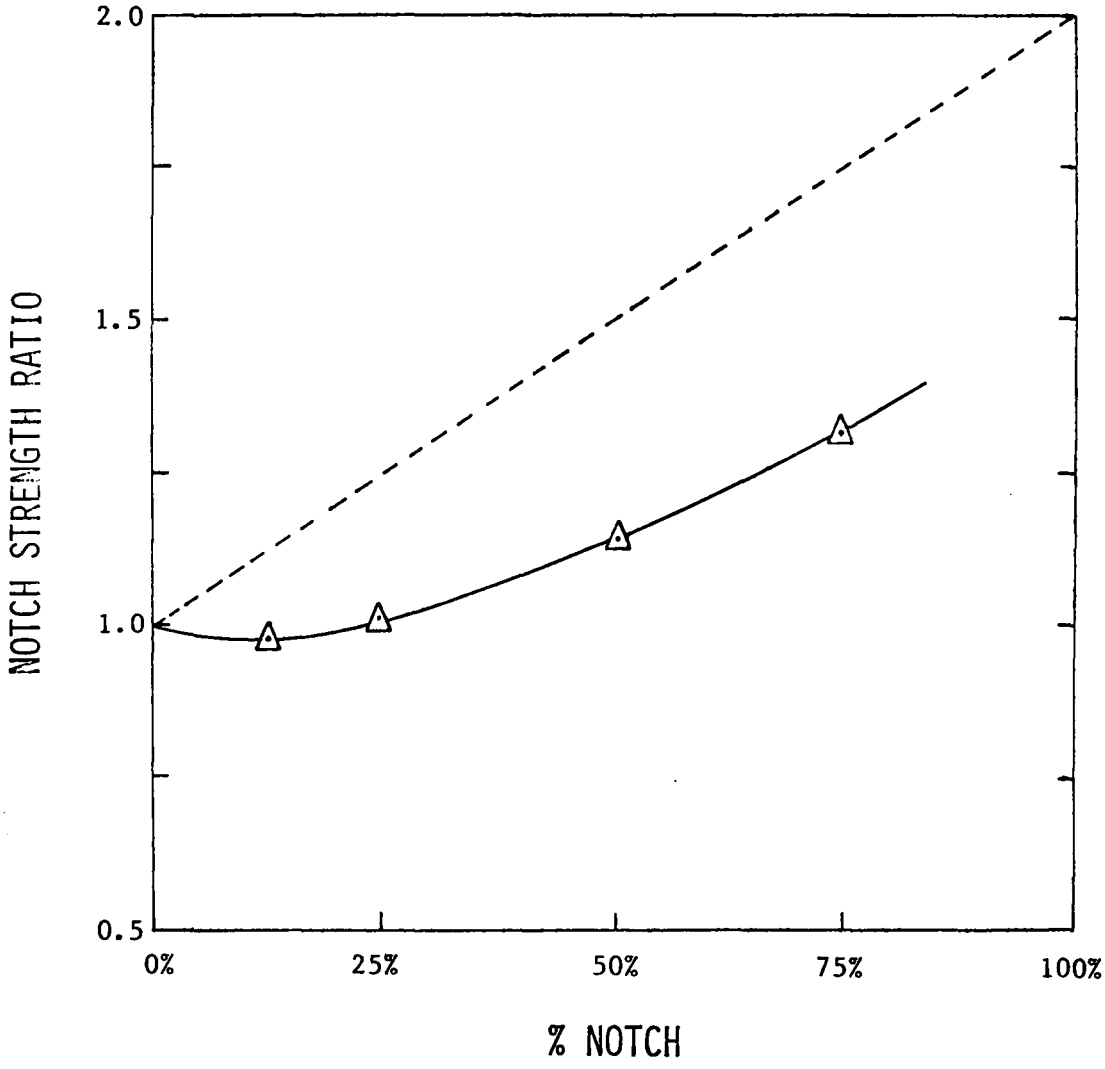

Figure 8. The effect of notch depth on notch strength ratio.

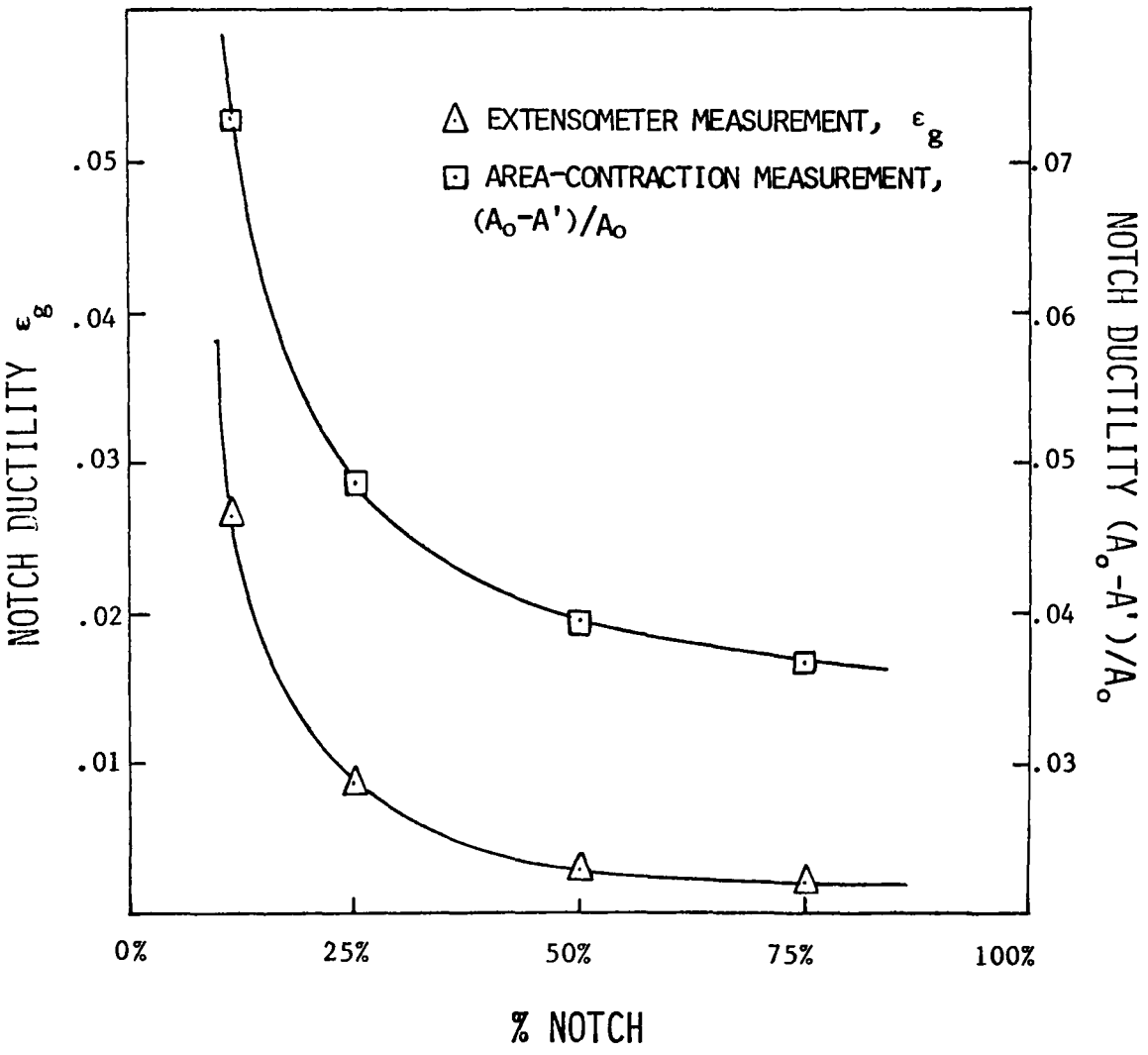

Figure 9. Dependence of notch ductility upon notch depth.

tional transverse strain gage employed by previous investigators[12,16,17]. Despite their different magnitude, both parameters show the tendency for decreasing ductility with respect to increasing notch depth. Note that the notch ductility for a 12.5% notch is about twice that for a 25% notch. This explains why a 12.5% notch induced little or no increase in the notch strength ratio as seen in Figure 8. It is apparent that the direct strain gage measurement can be used as a measure of notch ductility. From Figure 10, it is seen that a straight line relationship exists between ε_g and ε_a, where ε_a denoted the area-contraction measurement $(A_o-A')/A_o$ and ε_g is as defined earlier. The equation of the straight line can be written as follows:

$$\varepsilon_g = \frac{2}{3} (\varepsilon_a - 0.035) \qquad (6)$$

It appears that the ε_g measurement is not as sensitive as the ε_a measurement below a critical range of notch ductility (viz. 0.035, the intercept on X-axis). This is probably due to the fact that an extensometer with one inch gage length cannot detect the localized notch-blunting effect very accurately below this critical range of 0.035, but the stage micrometer technique detects the localized notch contraction even when general yielding across the cross-section has not occurred. If an extensometer with 1/4 inch or less gage length were used, this insensitivity might be eliminated.

The dependence of triaxiality on the notch depth is shown in Figure 11. Like all other metals and alloys, the triaxiality of aluminum alloy 2024-T351 increases with increasing notch depth.[2,3] It is this

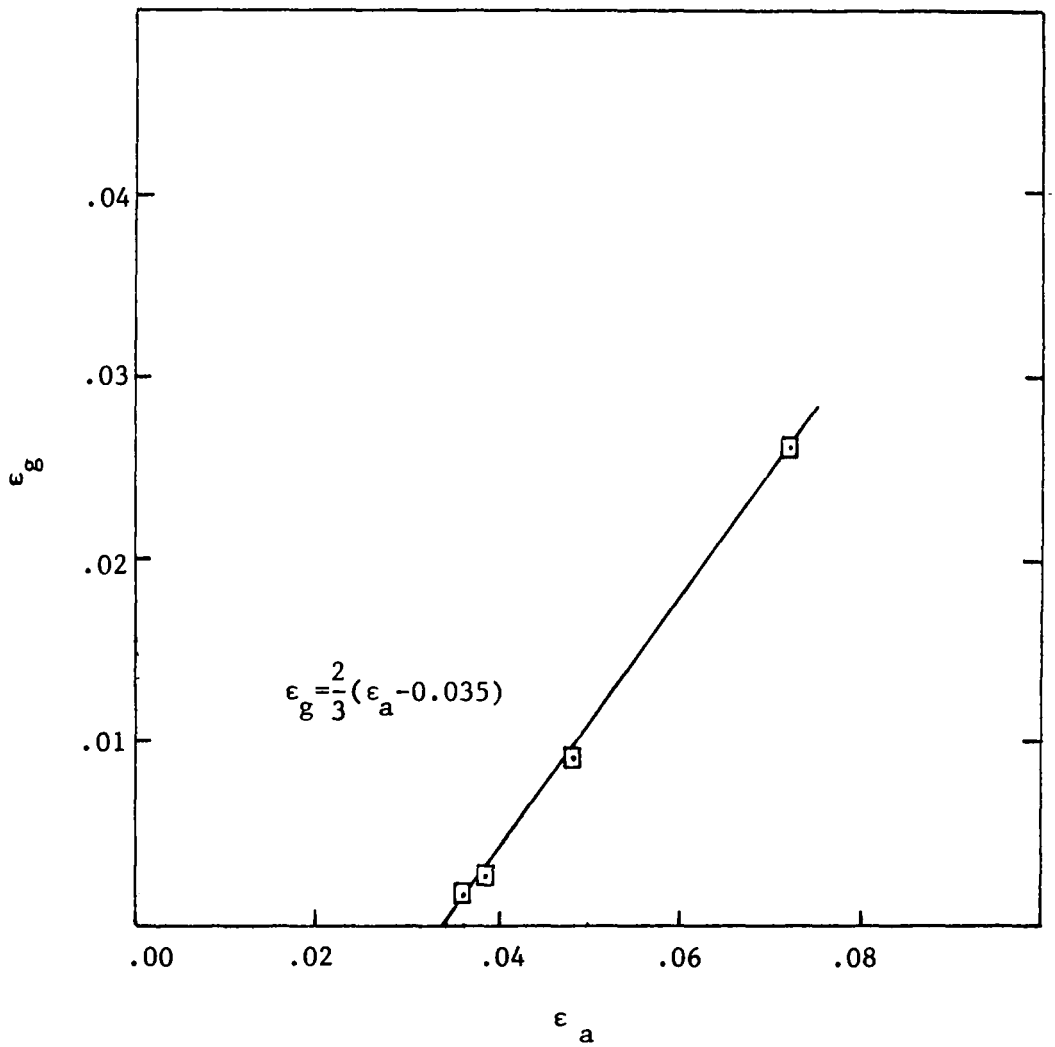

Figure 10. Plot of ε_g versus ε_a.

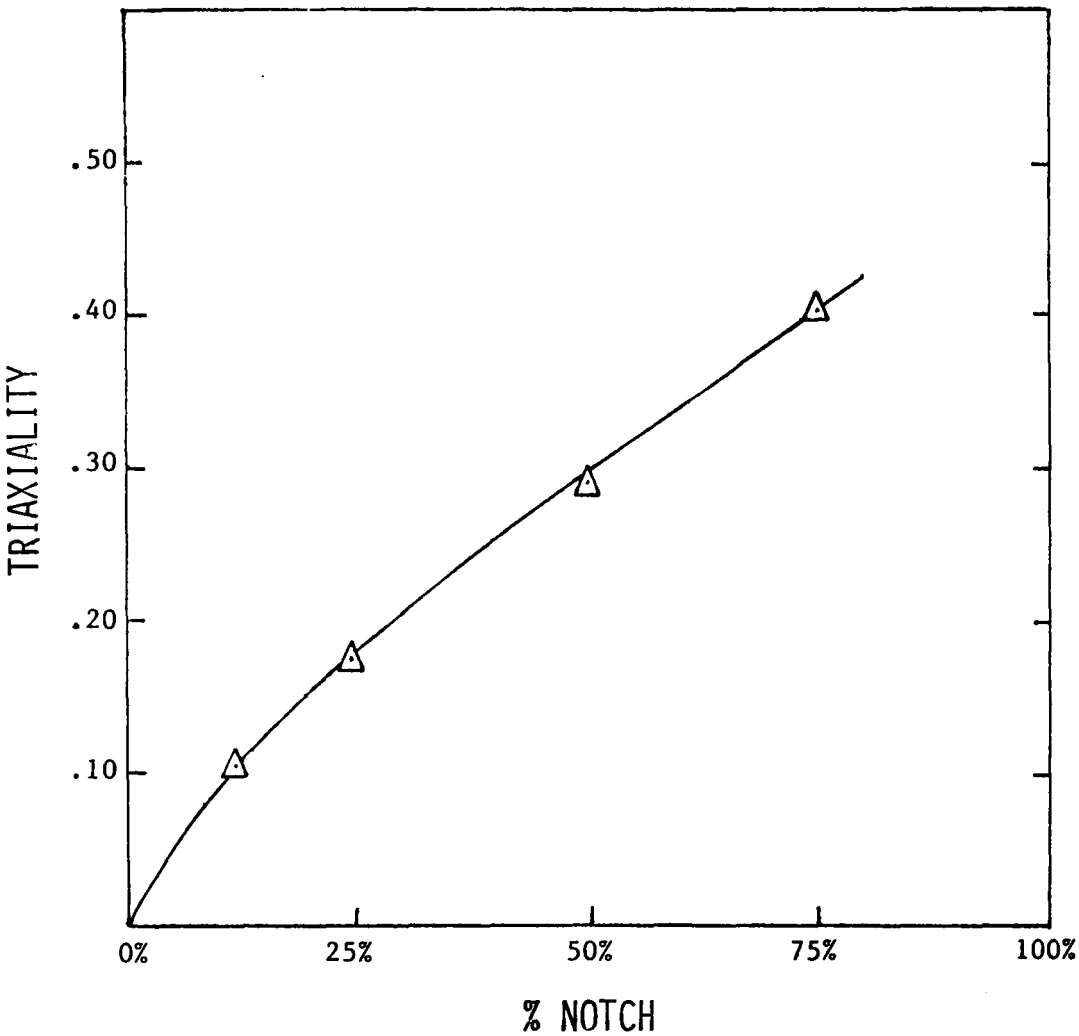

Figure 11. Dependence of triaxiality on notch depth.

triaxiality which increases the notch strength and decreases the notch ductility as notch depth increases[2,3,12,16,17].

Scanning electron fractographs of notched tensile ruptures are shown in Figure 12, Figure 13, and Figure 14. The fracture surface shown in Figure 12 is from the center region of a 50% notched specimen. It shows three kinds of fracture mode: dimple rupture, cleavage and quasi-cleavage at J, K, and L, respectively. These three types of fracture were always found in tensile rupture. In Figure 13, a well-defined yielding zone, G, near the root of the notch, R, is shown on the picture. This yielding zone is believed to be caused by initial crack advance during loading due to high stress concentration at the root of the notch. The depth of this yielding zone, d, as measured for different notch depths is shown in Table III. The yielding-zone depth, $\bar{d}$, is the average value of the measurements taken from four seperate sections 90^{o} apart on the fracture surface. The stress concentration factors tabulated are those from the data collected by Peterson[15]. It appears that, in the 75% notched specimen, the triaxiality is so large that it overcomes the effect of stress concentration and lowers the $\bar{d}$ value.

Figure 14 shows two sets of stereo pairs; one for the edge region of a 50% notched specimen, the other for the center region of a 75% notched specimen. Use of a stereo viewer with these pairs will allow the reader to observe the three-dimensional nature of the rupture surfaces.

B. The Effect of Fatigue Precracking

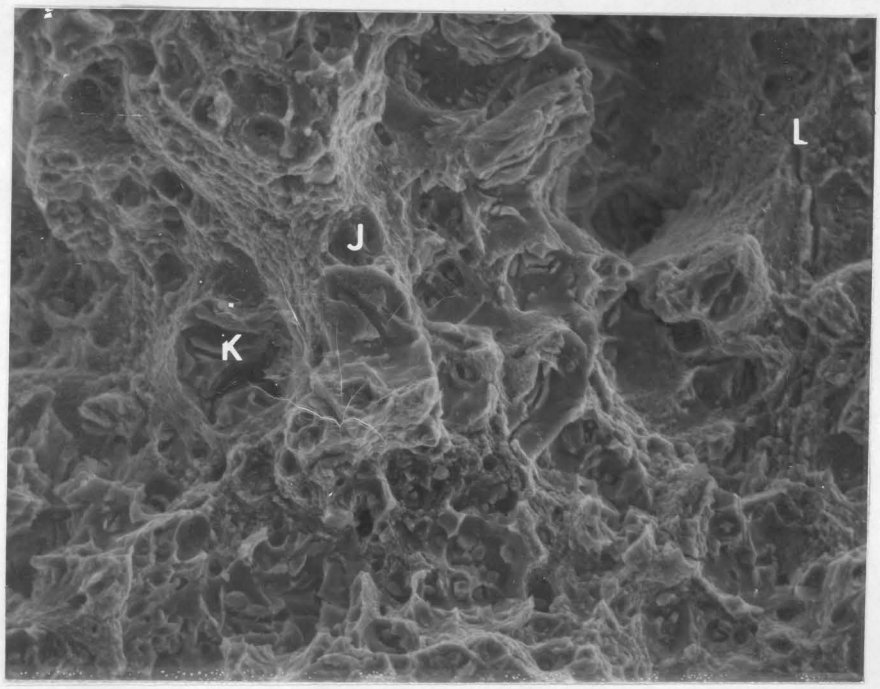

Figure 12. Fracture surface center region of 50% notched tensile specimen. Dimpled rupture is shown at "J". Cleavage of $CuAl_2$ particles is shown at "K". Quasi-cleavage is at "L". Scanning electron micrograph. 500X.

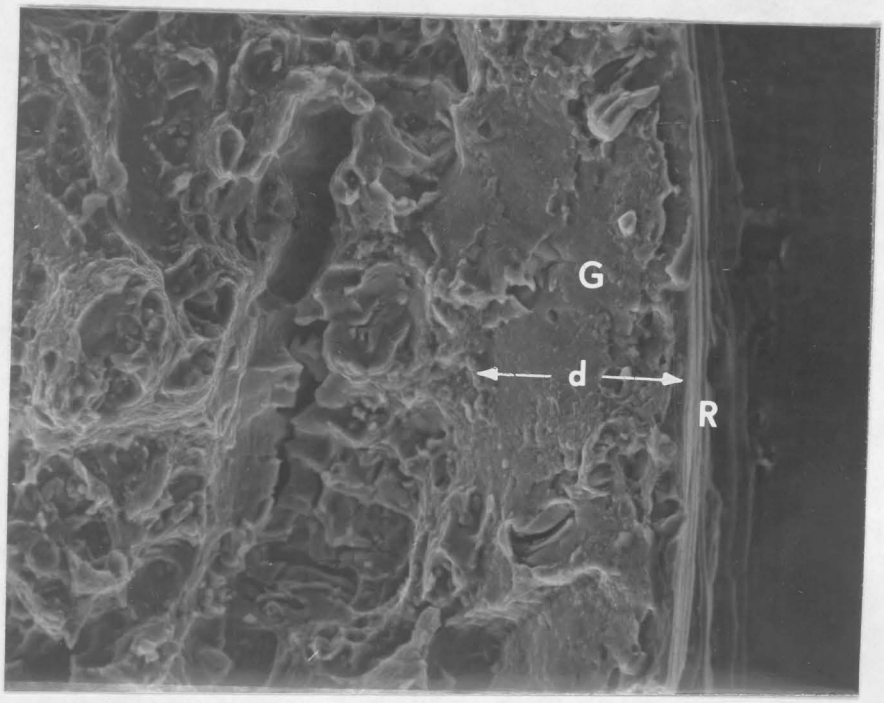

Figure 13. Fracture surface at the edge of 50% notched tensile specimen. The notch root is at "R" and "G" represents the yield zone. The depth of the yield zone is "d". Scanning electron micrograph. 500X.

TABLE III

Variation of Yielding-Zone Depth

% Notch	12.5%	25%	50%	75%
$\bar{d}$ (micron)	54.1	57.2	76.2	50.8
Stress Conc. Factor	5	6	6.65	6.2

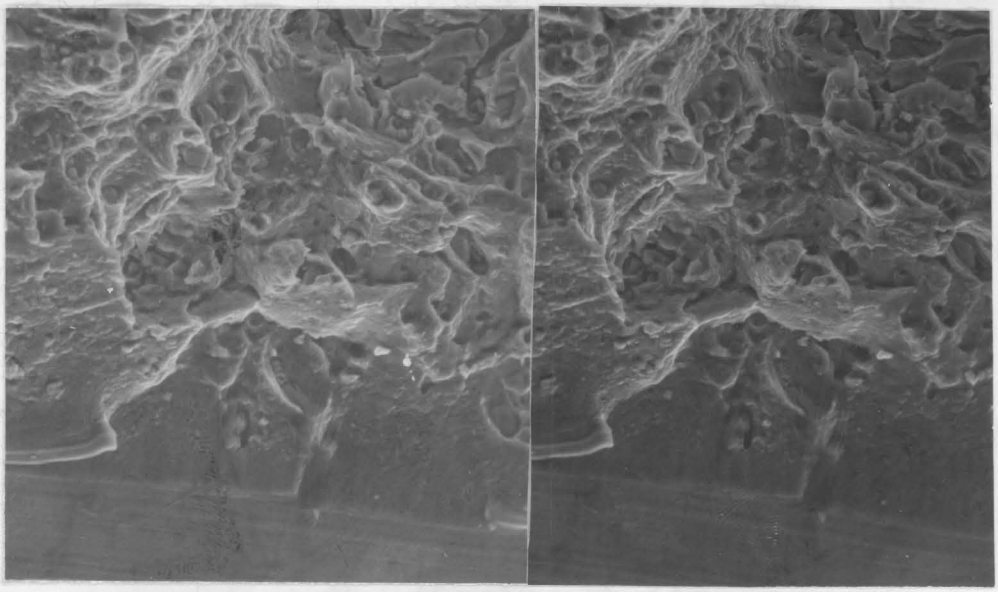

(a) Edge of 50% notched specimen

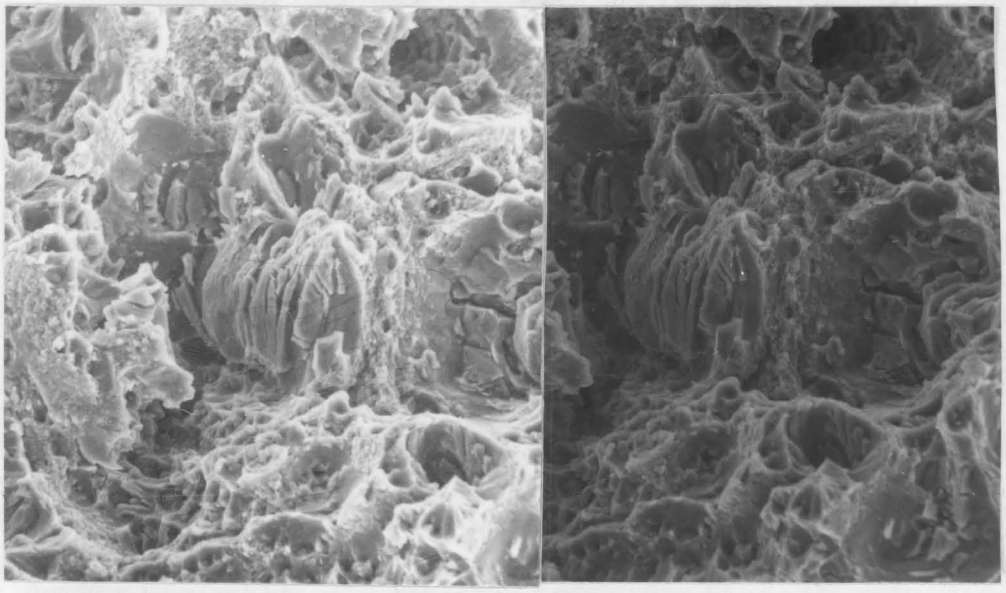

(b) Center of 75% notched specimen

Figure 14. Stereopairs of notched specimen after rupture. Scanning electron micrographs. 500X.

It was believed that fatigue cracks produced at the base of the machined notches would represent the sharpest possible notch, i.e. notch radius less than 0.0005 inch. To determine how this might affect notched tensile behavior, several specimens were pre-fatigued under various conditions prior to tensile testing. Table 4 lists the notch tensile strength of specimens which were fatigue-precracked under a reversed bending stress of 11.4 ksi. This stress exceeds the reported fatigue strength limit of 20 ksi for 2024-T351[40] if one assumes a notch fatigue factor of 1.80. In other words, with a stress of 11.4 ksi acting on the notch root of the specimen, the effective fatigue stress is 20.5 ksi. This is slightly more than the reported fatigue strength limit of 20 ksi at 5.0×10^8 cycles. With a value of 20.5 ksi for the fatigue stress, it would be expected that fatigue cracks would eventually be formed; especially, under the action of a salt-water corrosive environment. Three testing conditions were used in the fatigue-precracking procedure: (1) air fatigue, (2) salt water corrosion fatigue, and (3) room temperature prestraining followed by salt-water fatigue precracking. Prestraining was applied to determine the importance of residual stresses at the tip of the notch due to machining. Prestraining consisted of loading the notched specimen in the Instron machine to 6500 lb and then unloading again. In most cases, this induced about 0.003" of permanent longitudinal deflection across the notch.

The results shown in Table IV and Figure 15 demonstrate the relationship between the notch strength ratio and fatigue-precracking time for each testing condition. It appears that fatigue-precracking at a

TABLE IV

N.T.S. of Fatigue-Precracked Specimens under Reverse Bending Stress of 11.4 ksi

Specimen Number	Running Time (min)	Testing* Condition	N.T.S.	N.S.R.
1-13	20	S.W.	81420	1.169
1-15	20	S.W./P.S.	79386	1.140
1-10	40	A.	79700	1.145
1-9	40	S.W.	80250	1.153
1-16	40	S.W./P.S.	79100	1.136
1-14	60	S.W.	79450	1.140
1-12	80	A.	81284	1.168
1-11	80	S.W.	82060	1.178
1-17	80	S.W./P.S.	78460	1.127
1-18	0	P.S.	81700	1.174
1-6	0	-	80360	1.155

* S.W. - 3% salt-water corrosion

A. - Air atmosphere

S.W./P.S.-Prestraining followed by 3% salt-water corrosion

P.S. - Prestraining to 0.003" of permanent strain.

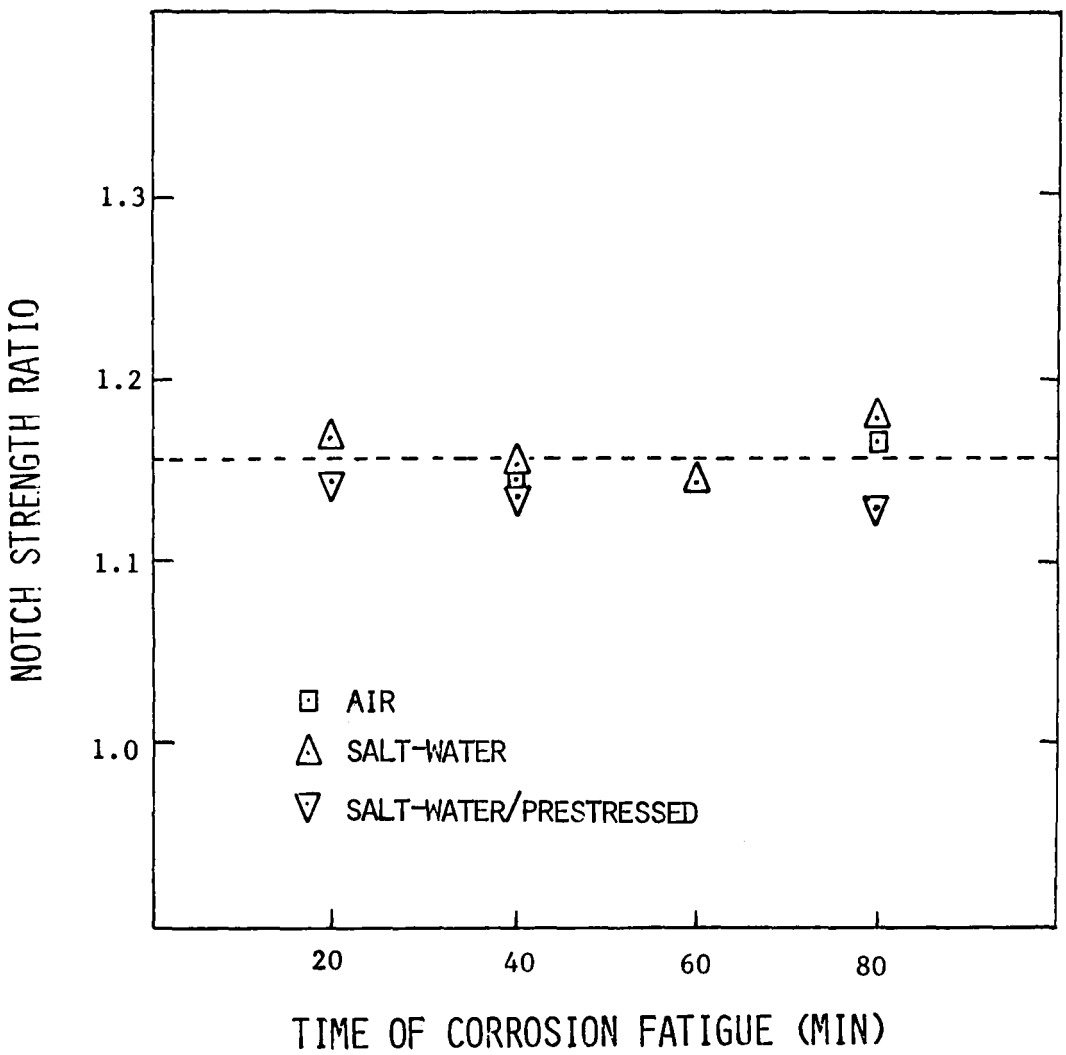

Figure 15. Dependence of notch strength ratio on the time of corrosion fatigue-precracking.

nominal stress of 11.4 ksi does not affect the notch strength characteristics, although the expected result would be a decreasing notch strength ratio with increasing prior fatigue.

An interesting new phenomenon was noted, however, from the tests reported in Table IV and Figure 16. When the strain-gage notch ductility, ε_g, was plotted as a function of fatigue time at 11.4 ksi in 3% salt-water for 50% notched samples, the results shown in Figure 16 were obtained. These results indicate an increase in notch ductility with increasing corrosion fatigue, whereas a decrease in notch ductility might have been expected due to the expected increase in notch depth. The reason for this behavior is the development of corrosion-fatigue cracks which run longitudinally along the specimen length from the notch root. The early stages of formation of these longitudinal cracks is shown in the macroscopic views of two fatigue-precracked tensile rupture specimens in Figure 17. Both specimens were pre-fatigued for 80 minutes at 11.4 ksi in 3% salt-water solution and then pulled to fracture. Figure 17(a) shows a specimen which was not prestrained; Figure 17(b) shows one which was prestrained. Note from these figures at the arrows that the longitudinal cracking shows up as a ridge which rises from the notch root at some locations. It forms a depression at the notch root at other locations, since these cracks move both directions from the notch root and the final normal rupture crack during tensile fracture apparently can choose to move to either of the fatigue crack tips. The fracture appearance reveals a lesser degree of longitudinal cracking for the prestrained specimen than for the non-prestrained specimen. It is

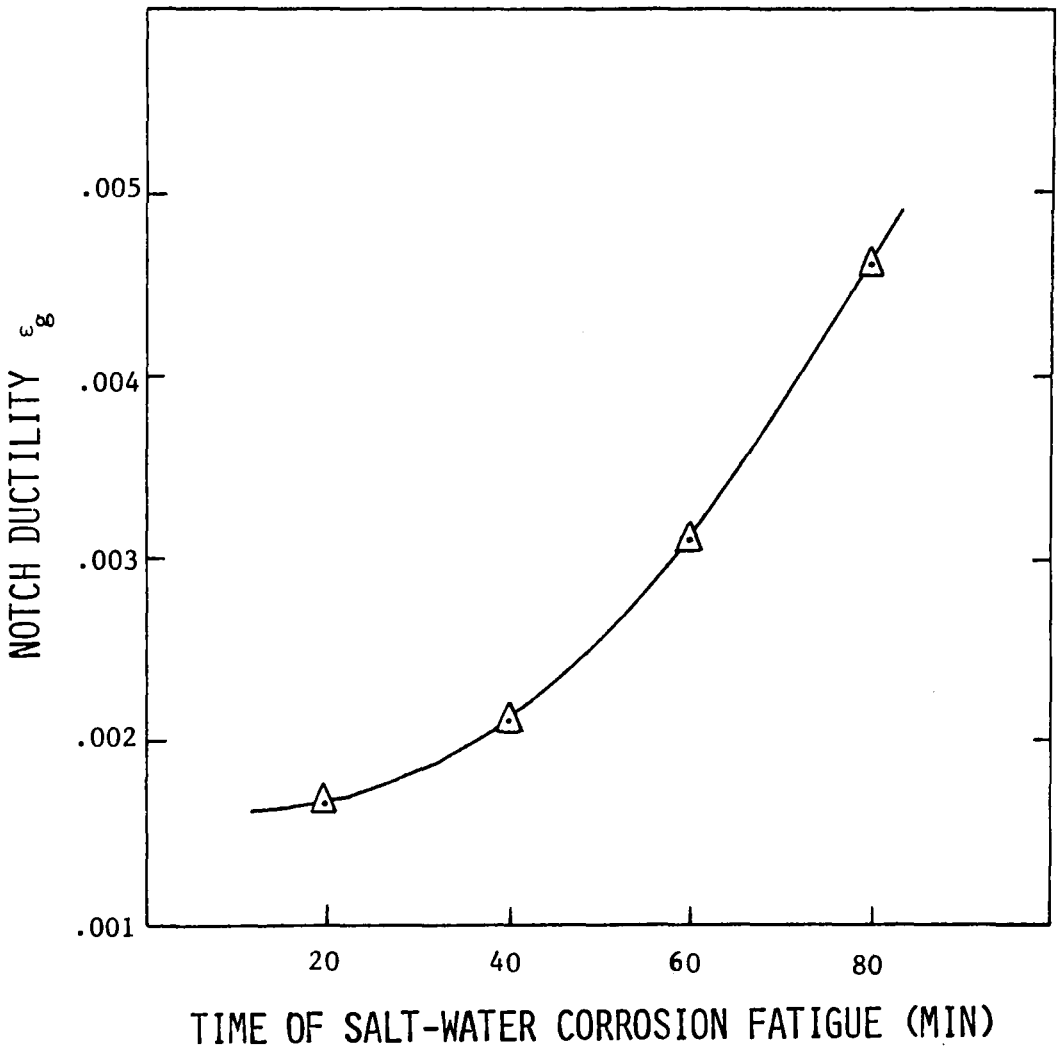

Figure 16. Effect of corrosion time on notch ductility.

(a) Non-prestrained

(b) Prestrained

Figure 17. Fracture appearance of prestrained and non-prestrained specimens pulled apart after 80 min. salt-water corrosion fatigue-precracking at 11.4 ksi norminal stress. 5X.

believed that fatigue cracks propagate into a longitudinal direction parallel to the specimen axis. However, due to relieving of residual stresses at the notch tip, the formation of sub-cracks in the prestrained specimen was restricted to only one direction. Also, the rate of crack propagation was slower in the prestrained specimen as compared to that in the non-prestrained specimen.

Figure 18 shows this behavior of a specimen which was prestrained to 6500 lbs and subjected to fatigue testing for 2.3×10^7 cycles, and subsequently pulled apart on a tensile machine. Again, fatigue cracks were found to be propogating in the longitudinal direction. In addition, shallow and apparently non-propagating cracks normal to the direction of loading were found surrounding the fracture surface. One of these shallow transverse cracks is seen at the arrow of Figure 18. The extent to which the longitudinal cracks can propagate during corrosion fatigue is readily seen in this figure. The maximum length was measured to be 3 mm.

It is concluded that under this low cyclic stress, a fatigue crack does not propagate in the notch plane, i.e., transverse cracks even in the presence of a 3% salt-water solution. In this regard, other investigators have found that a critical cyclic stress is required to propagate such transverse cracks in some aluminum alloys.[6,45,46] This provides an explanation for the failure of notch strength ratios to be affected by prior corrosion fatigue at 11.4 ksi. Furthermore, it is now clear that the effect of the longitudinal corrosion fatigue cracks is to provide for blunting of the original notch and thus increase notch ductility as was shown in Figure 16.

Figure 18. Fracture topology of prestrained and fatigue-precracked specimen after 23 million cycles at 11.4 ksi. Transverse crack is shown at arrow. 4.2X.

In order to better determine the location of the origin of these transverse cracks, the two specimens shown in Figure 18 were examined in the scanning electron microscope, especially in the region of the notch root. Representative notch root regions are shown in Figure 19 at 500X. In both specimens, the notch root is at the bottom of the figure and the cracks going downward into the paper are the longitudinal cracks. It is significant to note that these crack surfaces are quite faceted and brittle in nature and suggest intergranular cracking. It should also be noted that the origin of these longitudinal cracks is about 20 microns inside the original notch root.

C. The Effect of Corrosive Environment on Fatigue Properties

The failure life of 2024-T351 was determined under four different conditions and the results are shown in Table V and Figure 20. Also shown are the notched air fatigue data of Lyst of ALCOA Research Laboratory, ARL.[47,48] The stresses shown are nominal stresses at the notch root without consideration of any stress concentration factors. The fatigue life determined during the course of this research was higher than the data of Lyst by a factor of four. In both cases, the tests were conducted in air on the reverse bending R-R Moore machine.

As previously noted, air fatigue may be considered to be corrosion fatigue promoted by the atmospheric factors of moisture, oxygen content, etc., and it has been proved in several investigations that moisture and oxygen content in the atmosphere will partially modify the fatigue life of aluminum alloys[27,30,31,49]. Despite possible differences in these atmospheric factors, only the notch factor need be considered in analyzing

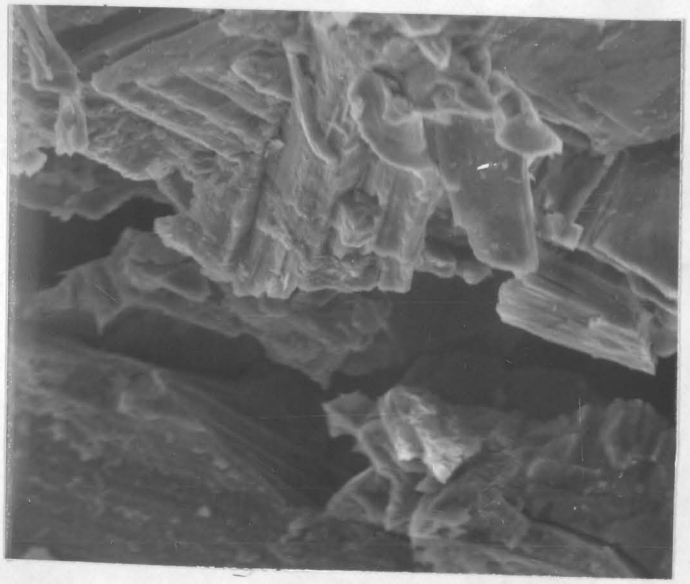

(a) Non-prestrained

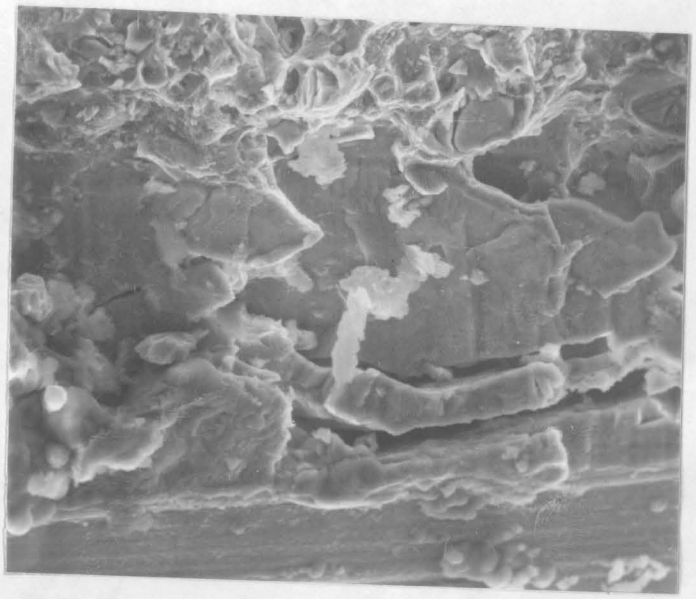

(b) Prestrained

Figure 19. Microscopic view of the edge of specimens pulled in tension after 80 minutes salt-water corrosion fatigue at 11.4 ksi. Scanning electron micrographs. 500X.

TABLE V

Notched Fatigue Properties of 50% Notched Aluminum Alloy 2024-T351

Specimen Number	Testing* Condition	Nominal Stress (ksi)	No. of Cycles to Failure
2-5	S.W.	17.1	1.95×10^5
2-6	Air	17.1	$> 1.70 \times 10^8$
2-7	S.W./P.S.	17.1	7.31×10^6
2-1	S.W.	22.9	5.02×10^4
2-2	S.W./P.S.	22.9	4.03×10^5
2-3	Air	22.9	2.38×10^5
2-16	Air/P.S.	22.9	7.70×10^5
2-10	S.W./P.S.	25.7	1.22×10^5
2-11	Air	25.7	1.05×10^5
2-12	S.W.	25.7	2.52×10^4
2-17	Air/P.S.	25.7	3.77×10^5

* S.W. - 3% salt-water corrosion

S.W./P.S. - Prestraining followed by 3% salt-water corrosion

Air /P.S. - Air fatigue after prestrained.

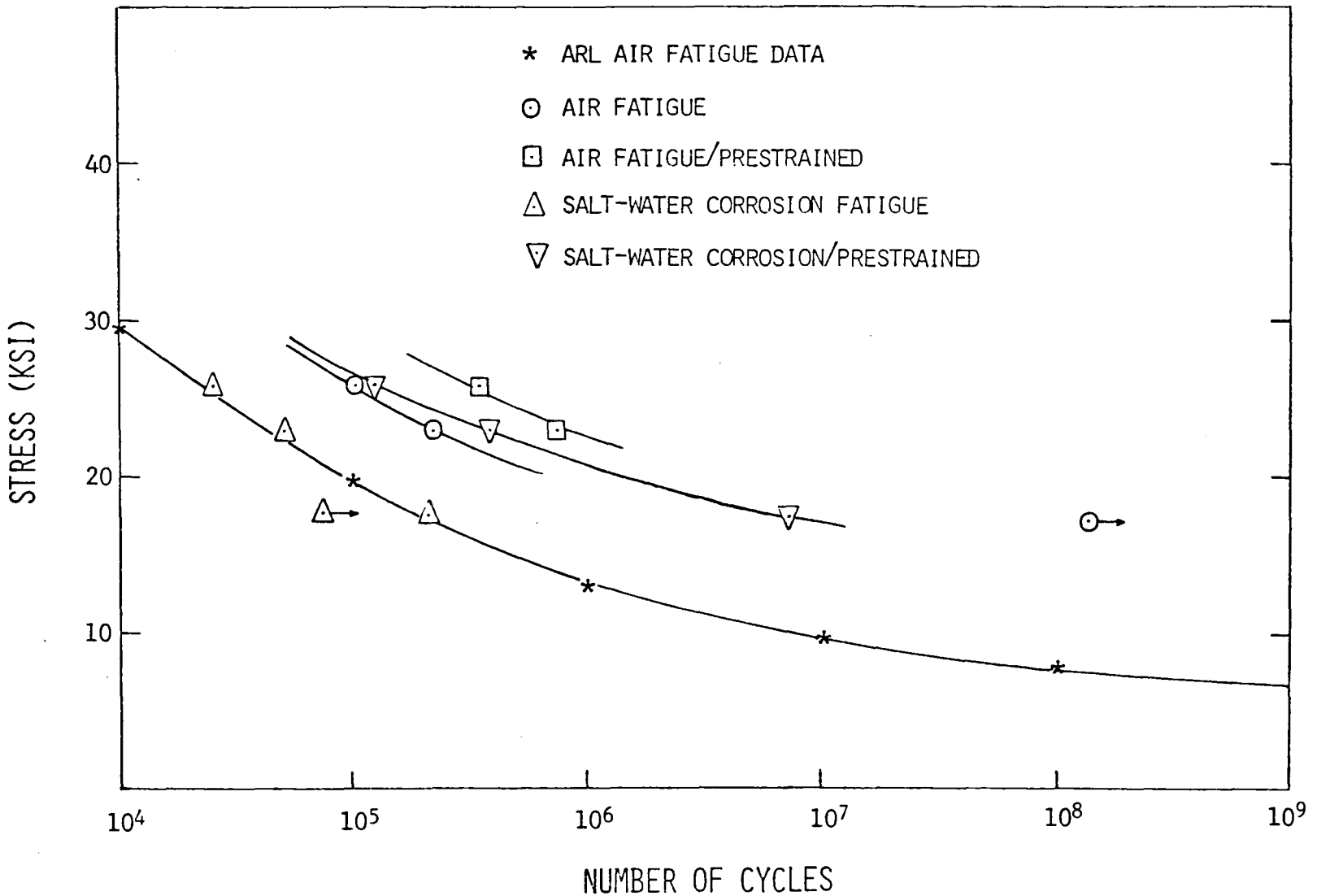

Figure 20. Notched-fatigue properties of aluminum alloy 2024-T351

the cause of the observed differences in fatigue life. In equation 3, the notch sensitivity q, was expressed as a function of stress concentration factor, K_t, and notch fatigue factor, K_f. According to Peterson[8], the value of q approaches a constant value of 0.18 as notch radius, r, falls below some critical value, i.e., in the range of very sharp notch. Thereafter, K_f is only a function of K_t and increases with K_t. The value of K_f of specimens with a notch radius of 0.0005 inch which is the notch radius of the specimens used by Lyst is larger than that of specimens with a notch radius of 0.003 inch the value used in these tests. In other words, the difference in notch radius accounts for the different fatigue life observed between these tests and those of Lyst. Allery and Birkbeck[50,51] have also verified such difference.

The results in Figure 20 also show that the effect of a 3% salt solution on the notched fatigue life of 2024-T351 alloy above about 20 ksi is to decrease the fatigue life by a factor of about four, thus providing agreement between the air fatigue data of Lyst of ARL and the present salt-water corrosion fatigue results. This suggests the possibility that one of the effects of salt-water corrosion was to provide rapid sharpening of the notch root to below the critical value for a sharp notch. It is not known, however, what effect salt-water corrosion would have had on the ARL data.

At a stress of 17.1 ksi, it is noted from Figure 20 that the effect of salt-water corrosion is to decrease fatigue life by more than a factor of 100, since the air fatigue specimen did not fail even after 170 million

cycles. In order to observe more closely the origin of fatigue crack formation for these two cases, the air fatigue specimen was sectioned radially in half using a low-speed diamond saw and hand polished so as to reveal the profile of the notch root area. A specimen fatigued in salt-water for only five minutes at 17.1 ksi was also sectioned and polished. Scanning electron micrographs of the air and corrosion fatigue root areas are shown at 500X in Figures 21 and 22, respectively.

Figure 21 shows that only one fatigue crack was formed after 7 days of high speed cyclic stress loading in air. This crack propagates at about 45 degrees to the notch plane and has achieved only about 0.002 inch depth. Figure 22 shows that more than one fatigue crack was formed at the root of the notch when the test was conducted in a salt-water environment for a period of only 5 minutes. The cracks in this figure propagate in the notch plane and were found to achieve about 0.0125 inch depth. In other words, the depth of crack for 5 minutes salt-water corrosion fatigue at 17.1 ksi is about six times greater than that for 7 days air fatigue. It is clear that the severe effect of salt-water corrosion at 17.1 ksi is related to the ease of initiation of a crack in the notch plane of sufficient size to begin propagating. While this critical size for 17.1 ksi is not precisely known, it would appear to be greater than 0.002 inches for the notch conditions employed herein. One interesting feature found in these two specimens which has not been previously reported is that intermetallic compounds may be fractured ahead of the fatigue crack tip. This is readily seen at the arrow of Figure 21.

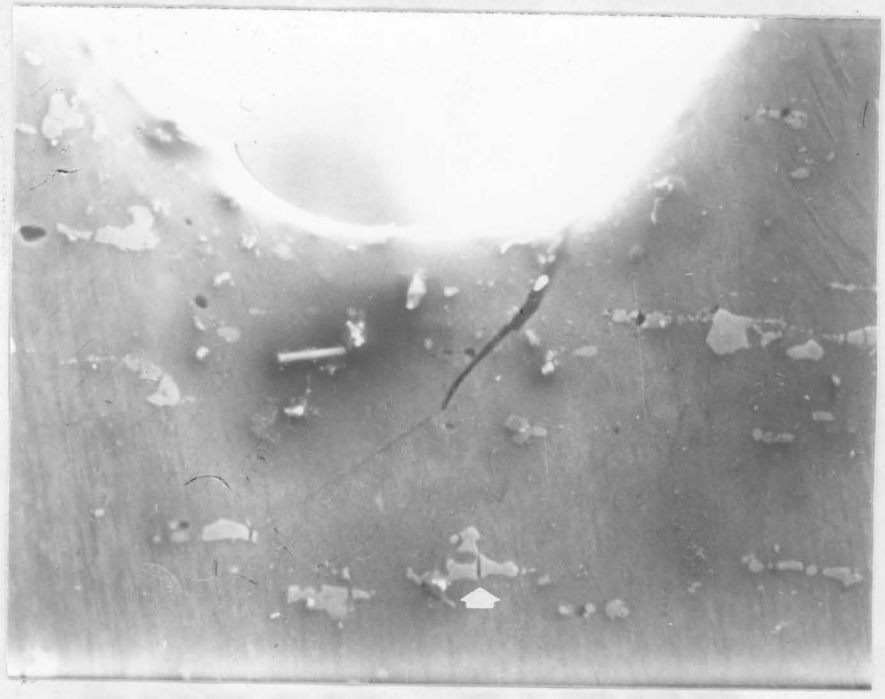

Figure 21. Fatigue crack at the notch root of an air fatigue specimen after 170 million cycles at 17.1 ksi. Scanning electron micrograph. 500X.

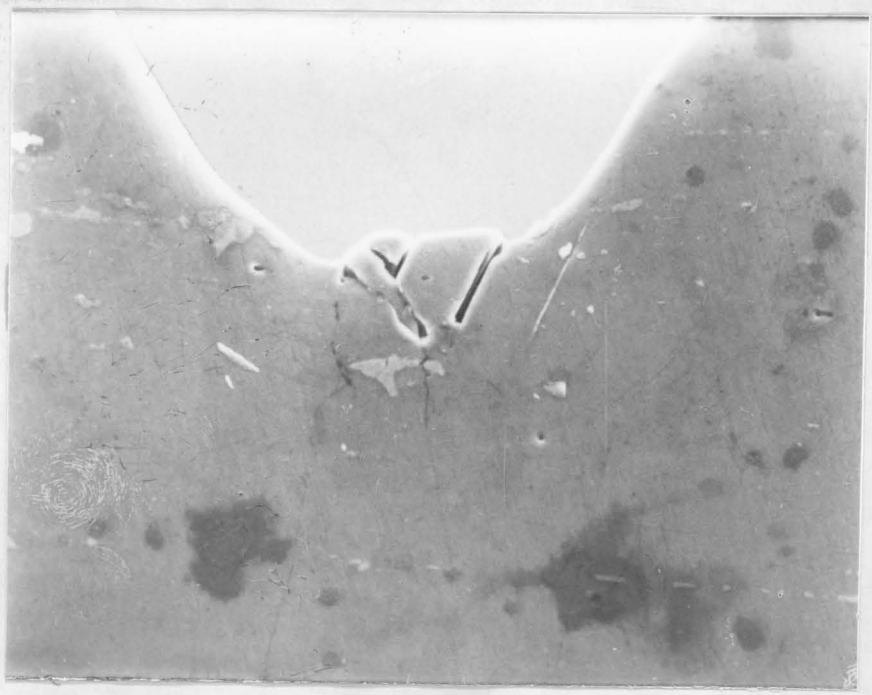

Figure 22. Fatigue cracks at the notch root of a salt-water corrosion fatigue specimen after 5 minutes fatigue at 17.1 ksi. Scanning electron micrograph. 500X.

Another distinctive result revealed by Figure 20 is that when both air and salt-water corrosion fatigue was conducted on prestrained specimens, the resulting S-N curve shifts to the right by a factor of more than four. There are at least two explanations for this. The first explanation is that the prestraining has provided for yielding at the notch root so that the sharpness at the root of the notch decrease and the notch-fatigue factor thereby reduced. The other explanation is that when the tensile load of prestraining is removed, a state of residual compression is induced at the notch root. For the latter explanation, an induced residual compressive stress of 5-7 ksi would explain the observed results.

The latter explanation is supported by the scanning electron micrographs of Figure 23 at 500X which show the notch root regions for both the non-prestrained and prestrained specimen after fatigue failure in salt-water at 25.7 ksi. Note that evidence of some longitudinal cracking is found in the prestrained specimen at the arrow, whereas none is seen in the non-prestrained specimen. Since this longitudinal cracking was found only at the low notch-plane stress of 11.4 ksi in corrosion fatigue, it follows that inducing low notch plane stresses by prestraining could induce longitudinal cracking in salt water at higher applied nominal stresses. The possibility that blunting of the crack tip during prestraining, however, must also be accepted as a plausible explanation, since a lowered stress concentration factor would also reduce the stress at the notch tip.

In order to determine the differences in fracture surface appearances

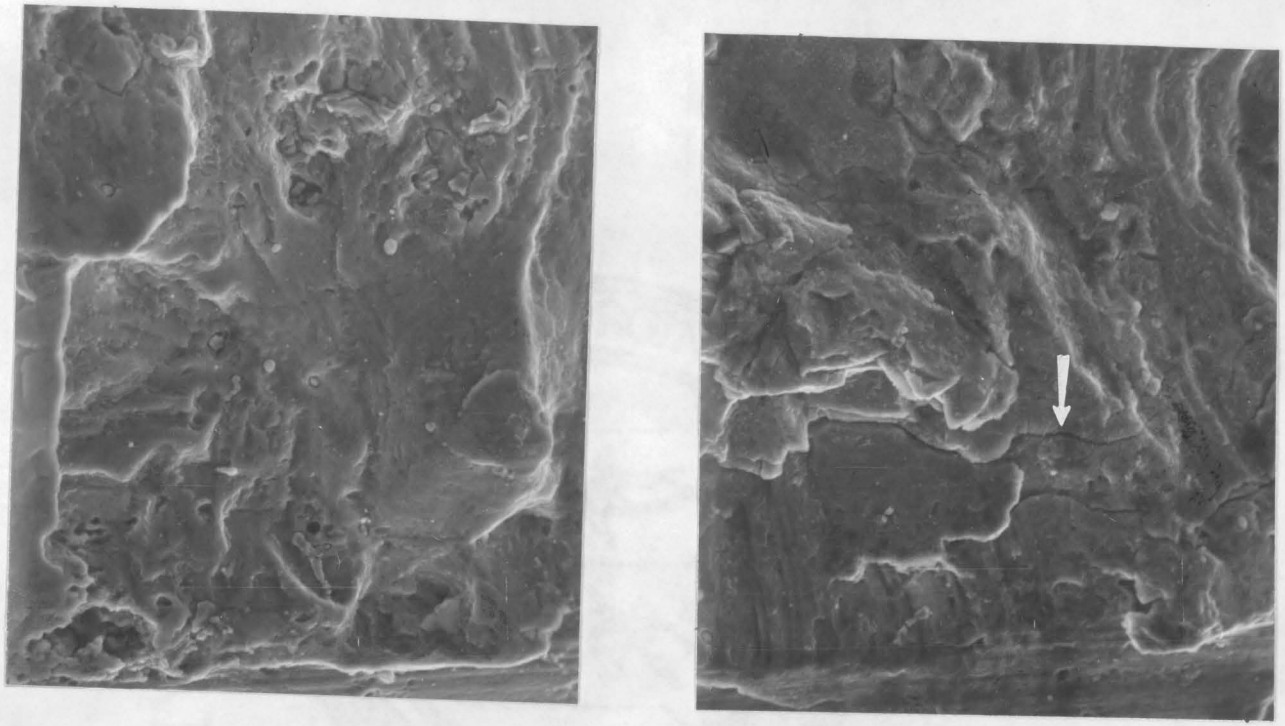

(a) Non-prestrained, 2.5×10^4 cycles.

(b) Prestrained, 1.22×10^5 cycles.

Figure 23. Comparison of fatigue fracture of prestrained and non-prestrained specimens after salt-water corrosion fatigue at 25.7 ksi. Arrow indicates longitudinal cracking. Scanning electron micrographs. 500X.

caused by salt-water corrosion fatigue, scanning electron micrographs of representative regions were obtained. Macroscopic views of two specimens failed in fatigue at 25.7 ksi are shown in Figure 24; Figure 24(a) shows the failure surface after air fatigue, and Figure 24(b) shows the fracture surface after salt-water corrosion fatigue. In each case, there is an initial zone of crack propagation at the notch root which appears bright to the eye and will be called the bright zone. These bright zones are seen at the arrows of Figure 24. In the center of each specimen is a rough, dull zone apparently characteristic of final rapid ductile rupture. As seen in Figure 24(a), a dark deposit forms in air fatigue between the two zones. The nature of this deposit is unknown, and its occurence has apparently not been reported elsewhere.

Scanning electron micrographs at 500X of each of the bright zones from Figure 24 are shown in Figure 25. The differences between the two surfaces are slight: some evidence of dimpled rupture is seen in each case, but there is considerably more secondary cracking in the case of salt-water corrosion fatigue. The bright appearance is apparently related to the occurence of relatively smooth regions mixed with the dimpled regions as shown at the arrows in Figure 25. At lower fatigue stresses, these flat regions were more predominant, and clear evidence of fatigue striations could be found. This is shown in Figure 26 at 500X for a stress of 17.1 ksi after salt-water corrosion fatigue.

As expected, the dull, central regions of each specimen in Figure 18 showed predominantly dimpled rupture. This is shown in Figure 27 at 500X. Except for the increased occurence of fractured intermetallic

(a) Air fatigue, 1.05×10^5 cycles.

(b) Salt-water corrosion fatigue, 2.52×10^4 cycles.

Figure 24. Macroscopic view of notched fatigue specimens after failure at 25.7 ksi. 5.2X.

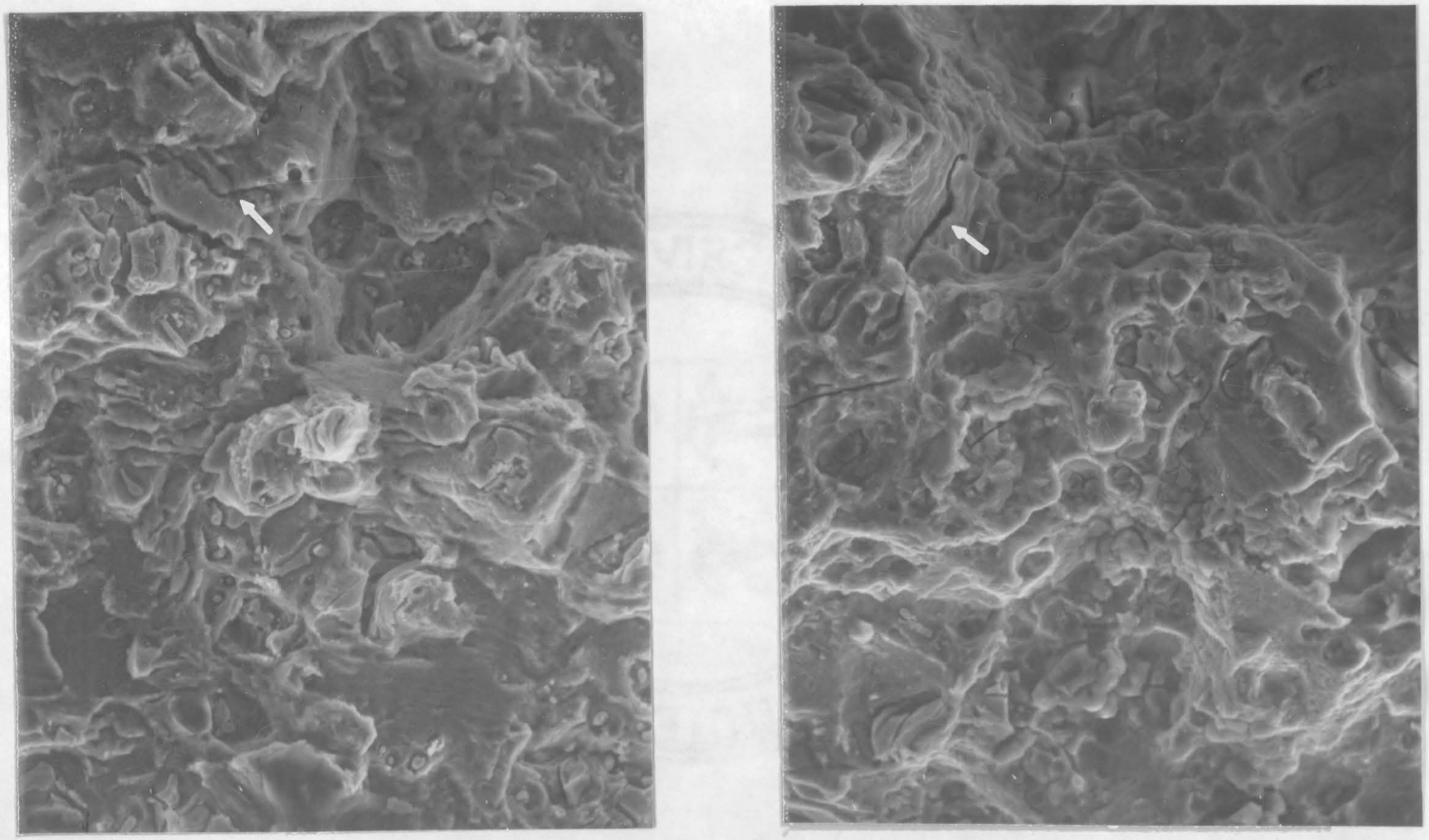

(a) Air fatigue

(b) Salt-water fatigue

Figure 25. Fatigue fracture appearance in bright zone. 25.7 ksi norminal stress. Arrow shows secondary cracking. Scanning electron micrographs. 500X.

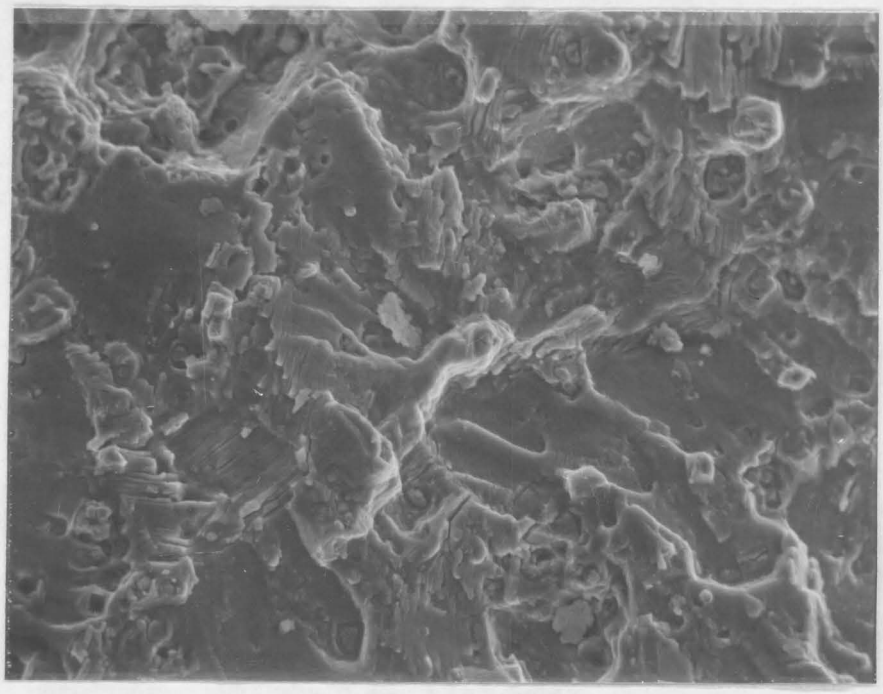

Figure 26. Striation fracture in bright zone of fatigue specimen after failure at 17.1 ksi during salt-water corrosion. Scanning electron micrograph. 500X.

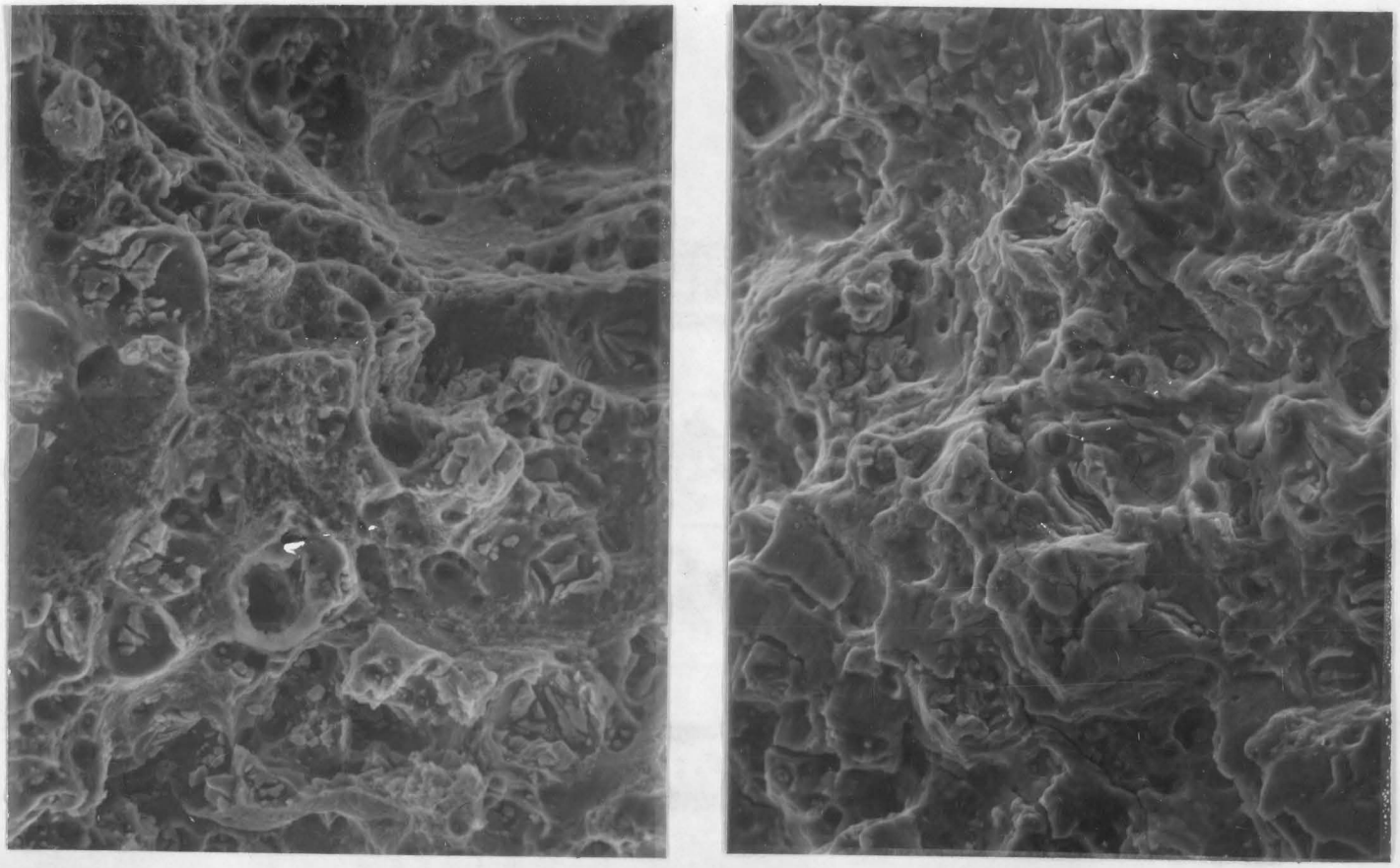

(a) Air fatigue

(b) Salt-water fatigue

Figure 27. Central region of specimens after fatigue rupture at 25.7 ksi. Scanning electron micrographs. 500X.

compounds, presumably $CuAl_2$, these dimpled regions resemble the fractographs obtained from tensile rupture specimens and reveal that final, rapid separation occurs by microvoid coalescence.

V. CONCLUSIONS

1. Notched tensile tests of 2024-T351 aluminum alloy have shown that high notch ductility for low notch depths results in a slight decrease in the notched strength ratio. This result is in agreement with other investigators of aluminum alloys and is different from that of steels where the notched strength ratio increases continuously with increased notch depth.
2. The use of a one-inch strain-gage extensometer across the notch has been shown to provide a resonable measure of notch ductility as measured by area contraction for notch ductilities greater than 0.035. The insensitivity of this measurement below 0.035 was related to inability to detect localized notch yielding using a one-inch extensometer.
3. Scanning electron microscopy revealed a yielding zone at the notch root after tensile rupture which was related to deformation associated with notch blunting during initial plastic flow due to stress concentration at the notch root.
4. During salt water corrosion fatigue at a low nominal stress of 11.4 ksi, notch ductility was found to increase with increasing corrosion fatigue. This was caused by a previously unreported tendency for cracks to initiate at the notch root which moved longitudinally to the specimen axis and acted to remove the stress concentration and triaxiality at the notch root.
5. A 3% salt water solution was found to decrease the fatigue life of 50% notched 2024-T351 aluminum by at least a factor of four. The

fracture surfaces as observed by scanning electron microscopy at stresses above 20 ksi did not reveal significant differences from air fatigue, and it was concluded that a significant part of the effect of salt water is the early and rapid sharpening of the notch root.

6. At a stress of 17.1 ksi, the effect of a 3% salt water on 50% notched fatigue specimens was to decrease fatigue life by a factor of more than 100. This was found to be the result of non-propagation of small cracks (about 0.002" long) formed in air fatigue, whereas salt water fatigue resulted in early formation of multiple fatigue cracks at the notch root.
7. Prestraining of 50% notched specimens to 6500 pounds prior to fatigue was found to increase both air and salt water corrosion fatigue life by about a factor of four. This was related to either a blunting of the crack tip during prestraining or the occurence of a residual compressive stress of 5-7 ksi on the notch plane at the notch tip.
8. Scanning electron microscopy has revealed that $CuAl_2$ intermetallic compounds may be fractured ahead of the fatigue crack and that fatigue striations are not readily observed at stresses above 20 ksi nominal stress at the notch root.

VI. BIBLIOGRAPHY

1. Lubahn, J. D., "On the Applicability of Notched Tensile Test Data to Strength Criterion in Engineering Design," Transactions ASME, January 1957, pp. 111-115.

2. Dana, A. W., Aul, E. L., and Sachs, G., "Effect of Triaxial Stress States on the Fracturing Characteristics of 24S-T Aluminum Alloy," NACA Tech. Note 1830, March 1949.

3. Dana, A. W., Aul, E. L., and Sachs, G., "Comparison of Notch Strength Properties of 24S-T, 75S-T, and 24S-T86 Aluminum Alloys," NACA Tech Note 1831, March 1949.

4. Walker, K., "The Effect of Stress Ratio during Crack Propagation and Fatigue for 2024-T3 and 7075-T6 Aluminum," ASTM STP 462, pp. 1-14.

5. Schwab, R. C., and Czyryca, E. J., "Effects of Notches and Saltwater Corrosion on the Flexural Fatigue Behavior of High-Strength Structural Alloys," ASTM STP 462, pp. 203-216.

6. Frost, N. E., "Notch Effects and the Critical Stress Required to Propagate a Crack in an Aluminum Alloy," Journal of Mechanical Engineering Science, Vol. 2, No. 2, 1960, pp. 109-119.

7. Frost, N. E., "Crack Formation and Stress Concentration Effects in Direct Stress Fatigue," The Engineer, September 30, 1955, pp. 464-467.

8. Peterson, R. E., Stress Concentration Design Factor, John Wiley, New York, 1970, pp. 1-30.

9. Grosskrentz, J. C., "Corrosion Fatigue of Aluminum Alloys, Critical Introduction," Corrosion Fatigue, NACE-2, 1971, pp. 451-453.

10. Duquette, D. J., "A Review of Aquous Corrosion Fatigue," Corrosion Fatigue, NACE-2, 1971, pp. 12-24.

11. Schwartzbart, H., and Brown Jr., W. F., "Notch-Bar Tensile Properties of Various Materials," Transactions ASM, Vol. 46, 1954, pp. 998-1020.

12. Sachs, G., and Lubahn, J. D., "Notched Bar Tensile Test Characteristics of Heat Treated Low Alloy Steels," Transactions ASM, Vol. 33, 1944, pp. 367-375.

13. Hetenyi, M., Handbook on Experimental Stress Analysis, John Wiley, New York, 1950.

14. Frocht, M. M., Photoelasticity, John Wiley, New York, 1951.

15. Peterson, R. E., Stress Concentration Design Factor, John Wiley, New York, 1970, pp. 30-80.

16. Sachs, G., and Lubahn, J. D., "The Effect of Triaxility on the Technical Cohesive Strength of Steels," Journal of Applied Mechnics, December 1945, pp. A241-A250.

17. Sachs, G., Lubahn, J. D., and Ebert, L., "The Effect of Notches of Varying Depth on the Strength of Heat Treated Steel," Transactions ASM, vol. 34, 1945, pp. 517-544.

18. Nelson, F. G., and Kaufman, J. G., "Plane Strain Fracture Toughness of Al Alloys at Room and Subzero Temperatures," ASTM STP 496, pp. 27-40.

19. Spahn, H., "Corrosion Fatigue in the Chemical Industry," Corrosion Fatigue, NACE-2, 1971, pp. 40-51.

20. Sachs, G., and Lubahn, J. D., "Effects of Notching on Strained Metals," Iron Age, Vol. 150, 1942, pp. 31-52.

21. Peterson, R. E., Metal Fatigue, Mcgraw Hill, New York, 1959, pp.301.

22. Head, A. K., "Fatigue Crack Propagation," Phil Magazine, Vol. 44, 1953, pp. 925.

23. Schijve, J., "Significance of Fatigue Cracks in Micro-Range and Macro-Range," ASTM STP 415, 1966, pp. 415-458.

24. Grosskrentz, J. D., and Shaw, G. G., "Microstructures at the Tips of Growing Fatigue Cracks in Aluminum Alloys," ASTM STP 415, 1966, pp. 226-246.

25. Laird, C., "The Influence of Metallurgical Structure on the Mechanisms of Fatigue Crack Propagation," ASTM STP 415, 1966, pp. 131-169.

26. Rice, J. R., "Mechanics of Crack Tip Deformation and Extension by Fatigue" ASTM STP 415, 1966, pp. 247-310.

27. Krupp, W. E., Hoeppner, D. W., and Walker, E. K., "Crack Propagation of Al Alloy in Corrosive Environment," Corrosion Fatigue, NACE-2, 1971, pp. 468-483.

28. Dieter, G. E., Mechanical Metallurgy, McGraw Hill, New York, 1961, pp. 320-323.

29. Hoeppner, D. W., "Corrosion Fatigue Considerations in Materials Selections and Engineering Design," Corrosion Fatigue, NACE-2, 1971, pp. 3-11.

30. Uhlig, H. H., Corrosion and Corrosion Control, Wiley, N.Y., 1963, pp. 112-150.

31. Shreir, L. L., "Non Ferrous Metals and Alloys," No. 4, Vol. 1, Corrosion, Newnes-Butterworths, 1976.

32. Beachem, C. D., and Pelloux, R. M., "Electron Fractography," Fracture Toughness Testing and Its Application, ASTM STP 381, pp. 210-245.

33. Beachem, C. D., and Meyn, D. A., "Fracture by Microscopic Plastic Deformation Processes," Electron Fractography, ASTM STP 436, pp. 68-88.

34. Hearle, Sparrow and Cross, The Use of Scanning Electron Microscope.

35. Rogers, H. C., "Tensile Fracture of Ductile Metals," Transaction AIMME, Vol. 218, June 1960, pp. 504.

36. Forsyth, P. J. E., and Ryder, D. A., "Some Results of the Examination of Aluminum Alloy Specimen Fracture Surfaces," Metallurgia, Vol. 63, March 1961, pp. 117-124.

37. Hull, D., Introduction to Dislocation, Pergamon Press, 1969, pp. 50-56.

38. Forsyth, P. J. E., and Ryder, D. E., "Fatigue Fracture Derived from the Microscopic Examination of Crack Surfaces," Aircraft Engineering, Vol. 32, 1960, pp. 94-96.

39. McMillan, J. C., and Hertzberg, R. W., "Application of Electron Fractography to Fatigue Studies," Electron Fractography, ASTM STP 436, 1968, pp. 89-123.

40. Aluminum Standard and Data, The Aluminum Association, 1976, pp. 15.

41. "Tension Testing of Metallic Materials," ASTM Annual Book, E 8, 1977, pp. 154-173.

42. Manual of Fatigue Testing, ASTM STP 91, 1949.

43. "Constant Amplitude Axial Fatigue Tests of Metallic Materials," ASTM Annual Standard, E466, 1977, pp. 536-540.

44. SEM/TEM Fractography Handbook, MCIC, December 1975, pp. 5-9.

45. Forsyth, P. J. E., "Proc. International Conference on Fatigue of Metals," Institution Mechanical Engineers, 1956, pp. 535.

46. Hyler, W. S., Lewis, R. A., and Grover, H. J., NACA Tech. Note 3291, 1954.

47. Lyst, L. O., "The Effects of Cold Working on the Fatigue Strength of Heat-Treated Aluminum Alloys : A Review of ARL Data and the Literature," Journal of Materials, Vol. 3, No. 4, December 1968, pp. 996-1017.

48. Lyst, J. O., "Effect of Stretching upon the Fatigue Strength of 2024-T4 Aluminum Alloys," Materials Research & Standards, Vol. 2, No. 9, September 1962, pp. 751-753.

49. Shreir, L. L., "Principles of Corrosion and Oxidation," Corrosion, No. 1, 1976, Newnes-Butterworths, Boston.

50. Allery, M., and Birkbeck, G., "Effect of Notch Root Radius on the Initiation and Propagation of Fatigue Cracks," Engineering Fracture Mechanics, Vol. 4, 1972, pp. 325-331.

51. Kuhn, P., and Hardrath, H. F., NACA Tech. Note 2805, 1952.

The vita has been removed from the scanned document

THE CORROSION FATIGUE BEHAVIOR OF NOTCHED 2024-T351 ALUMINUM

by

Steve A. Chang

(ABSTRACT)

Notched tensile tests and notched fatigue tests were performed at room temperature to study the corrosion fatigue behavior of aluminum alloy 2024-T351 in 3% salt solution.

Notched characteristics of aluminum alloy 2024-T351 were found to be the same as those of other high strength aluminum alloys. Triaxiality and stress concentration were the main factors in determination of the notch characteristics. A new definition of notch ductility was developed in this study and the results compared to the use of area-contraction ductility.

Air and 3% salt solution were used as the corrosive agents in the notched fatigue tests. Salt water corrosion was found to decrease the fatigue life to no more than one-fourth of the value for air fatigue. This was explained by the significant effect of salt water which sharpens the notch root rapidly at the early stage of the fatigue tests. However, this fatigue life during salt-water corrosion was decreased by a factor of more than 100 at a stress of 17.1 ksi. This enhanced effect of salt water was found to be the result of rapid propagation of small cracks which would not propagate in air fatigue.

At the nominal stress of 11.4 ksi, notch ductility was found to increase with increasing salt-water corrosion fatigue. This was caused by a tendency for cracks to initiate at the notch root and move parallel

to the specimen axis. This surprising result is the only known occurrence of this type of cracking.

The appearance of fractographs obtained by the scanning electron microscope was correlated with the fracture characteristics in both the notched tensile tests and notched fatigue tests.